Invited research article

The rise and fall of the Cretaceous Hot Greenhouse climate

Brian T. Huber[a,*], Kenneth G. MacLeod[b], David K. Watkins[c], Millard F. Coffin[d,e,f]

[a] Department of Paleobiology, MRC-121, Smithsonian Institution, Washington, DC 20013, United States
[b] Department of Geological Sciences, University of Missouri-Columbia, Columbia, MO 65211, United States
[c] Department of Earth & Atmospheric Sciences, University of Nebraska, Lincoln, NE 68588, United States
[d] Institute for Marine and Antarctic Studies, University of Tasmania, Private Bag 129, Hobart, TAS 7001, Australia
[e] School of Earth and Climate Sciences, University of Maine, Orono, ME 04469-5790, United States
[f] Woods Hole Oceanographic Institution, Woods Hole, MA 02543, United States

ARTICLE INFO

ABSTRACT

A compilation of foraminiferal stable isotope measurements from southern high latitude (SHL) deep-sea sites provides a novel perspective important for understanding Earth's paleotemperature and paleoceanographic changes across the rise and fall of the Cretaceous Hot Greenhouse climate and the subsequent Paleogene climatic optimum. Both new and previously published results are placed within an improved chronostratigraphic framework for southern South Atlantic and southern Indian Ocean sites. Sites studied were located between 58° and 65°S paleolatitude and were deposited at middle to upper bathyal paleodepths. Oxygen isotope records suggest similar trends in both bottom and surface water temperatures in the southern sectors of the South Atlantic and in the Indian Ocean basins. Warm conditions were present throughout the Albian, extreme warmth existed during the Cretaceous Thermal Maximum (early-mid-Turonian) through late Santonian, and long-term cooling began in the Campanian and culminated in Cretaceous temperature minima during the Maastrichtian. Gradients between surface and seafloor δ^{18}O and δ^{13}C values were unusually high throughout the 11.5 m.y. of extreme warmth during the Turonian-early Campanian, but these vertical gradients nearly disappeared by the early Maastrichtian.

In absolute terms, paleotemperature estimates that use standard assumptions for pre-glacial seawater suggest sub-Antarctic bottom waters were ≥21 °C and sub-Antarctic surface waters were ≥27 °C during the Turonian, values warmer than published climate models support. Alternatively, estimated temperatures can be reduced to the upper limits of model results through freshening of high latitude waters but only if there were enhanced precipitation of water with quite low δ^{18}O values. Regardless, Turonian planktonic δ^{18}O values are ~1.5‰ lower than minimum values reported for the Paleocene-Eocene Thermal Maximum (PETM) from the same region, a difference which corresponds to Turonian surface temperatures ~6 °C warmer than peak PETM temperatures if Turonian and Paleocene temperatures are estimated using the same assumptions. It is likely that warm oceans surrounding and penetrating interior Antarctica (given higher relative sea level) prevented growth of Antarctic ice sheets at all but the highest elevations from the late Aptian through late Campanian; however, Maastrichtian temperatures may have been cool enough to allow growth of small, ephemeral ice sheets. The standard explanation for the sustained warmth during Cretaceous Hot Greenhouse climate invokes higher atmospheric CO$_2$ levels from volcanic outgassing, but correlation among temperature estimates, proxy estimates of pCO$_2$, and intervals of high fluxes of both mafic and silicic volcanism are mostly poor. This comparison demonstrates that the relative timing between events and their putative consequences need to be better constrained to test and more fully understand relationships among volcanism, pCO$_2$, temperature ocean circulation, Earth's biota and the carbon cycle.

1. Introduction

Evidence for warm polar regions during the Cretaceous is well documented. Terrestrial plant assemblages and dinosaurs from polar latitudes of both hemispheres indicate mean annual and winter minimum temperatures much warmer-than-modern (Brouwers et al., 1987; Case, 1988; Case et al., 2000; Herman and Spicer, 1997; Olivero et al., 1991; Parrish et al., 1989; Parrish and Spicer, 1988; Rich et al.,

2002). Presence of champsosaur (a crocodile-like reptile) remains at ~72°N during the Turonian-Coniacian is consistent with mean annual temperatures of > 14 °C (Tarduno et al., 1998; Vandermark et al., 2007). Geochemical confirmation and refinement of temporal trends are provided by paleotemperatures inferred from foraminiferal oxygen isotope compilations (e.g., Cramer et al., 2009; Friedrich et al., 2012), fish teeth (Pucéat et al., 2007; Martin et al., 2014) and TEX$_{86}$ measurements derived from the composition of membrane lipids of marine Archaea (O'Brien et al., 2017).

The compilations of deep-sea benthic foraminiferal and bulk carbonate $\delta^{18}O$ data reveal that warming of the world's oceans to the mid-Cretaceous peak was gradual and spanned the early Albian through middle Cenomanian. Extremely warm temperatures (seafloor temperatures of > 20 °C at mid-bathyal depths) persisted from the late Cenomanian through Santonian, and then gradually returned to cooler values (~6–8 °C at mid–bathyal depths; ~1500–2500 m) during the Maastrichtian (Clarke and Jenkyns, 1999; Huber et al., 1995; Huber et al., 2011; Huber et al., 2002; Cramer et al., 2009; Friedrich et al., 2012). Oxygen isotopic records from surface dwelling planktonic foraminifera in the southern South Atlantic have been shown generally to parallel the deep-sea benthic $\delta^{18}O$ trends with highest planktonic $\delta^{18}O$ values during the late Aptian-early Albian and Maastrichtian "cool greenhouse" and lowest values during the Turonian-Santonian "hot greenhouse" (Huber et al., 1995, 2002; Barrera and Savin, 1999; Fassell and Bralower, 1999).

Extreme warmth during the mid-Cretaceous has been ascribed to high pCO$_2$ maintained by high fluxes from volcanic activity including increased oceanic crust formation, eruption of large igneous province (LIP), and high rates of subduction-related arc volcanism (Arthur et al., 1985; Barron and Washington, 1985; Crowley, 1991; Larson, 1991a; Coffin and Eldholm, 1994; Crowley and Berner, 2001; Van Der Meer et al., 2014). The buildup of atmospheric CO$_2$, palaeogeography, and warm Cretaceous oceans created conditions near the threshold for widespread deposition of organic-rich sediments under anoxic conditions, as demonstrated by the repeated occurrence of Oceanic Anoxic Events (OAEs) and their associated prominent carbon-isotope excursions documented from marine and terrestrial sequences (Ando et al., 2002; Arthur et al., 1988; Gröcke et al., 1999; Jahren et al., 2001; Jarvis et al., 2006; Jenkyns, 1980, 2010; Jenkyns et al., 2017). Globally expressed Cretaceous OAEs occurred during the early Aptian (OAE 1a; ~120 Ma) and at the Cenomanian/Turonian boundary (OAE 2; ~94 Ma) while regionally recognized events occurred during the early Albian (OAE 1b; ~111 Ma), late Albian (OAE 1d; ~100 Ma) and possibly late Coniacian-early Santonian (OAE 3; ~86 Ma). Two end-member models, one invoking reduced ocean circulation (stagnant ocean basins) and another invoking high plankton productivity and expansion of the oxygen minimum zone (productivity model), have been proposed to explain OAEs. Where on this spectrum the answer remains debated due to discrepancies between model predictions and empirical observations, and forcing mechanisms for OAEs remain poorly understood (Jenkyns, 2010). Regardless of triggering mechanisms, the burial of large amounts of organic carbon should have reduced pCO$_2$ and lowered temperatures globally.

At Falkland Plateau DSDP Site 511 (Fig. 1), planktonic foraminiferal $\delta^{18}O$ values from the Turonian are especially low, ranging at times to between −4.2 and −4.7‰. These values suggest upper ocean at ~60 °S paleolatitude was as warm as 29–32 °C assuming the standard ice-free values of −1‰$_{SMOW}$ applies for regional seawater $\delta^{18}O$ (Bice et al., 2003). The low planktonic $\delta^{18}O$ values (and resulting high paleotemperature estimates) have defied straightforward heat budget explanations. In the Bice et al. (2003) study, temperatures of ~30 °C were incompatible with model results unless the models use either improbably high pCO$_2$ levels (≥6500 ppm) or proscribed at least a 50% increase in oceanic poleward heat transport relative to earlier mid-Cretaceous conditions. Reducing calculated temperatures by invoking moisture balance changes that lowered seawater $\delta^{18}O$ was considered
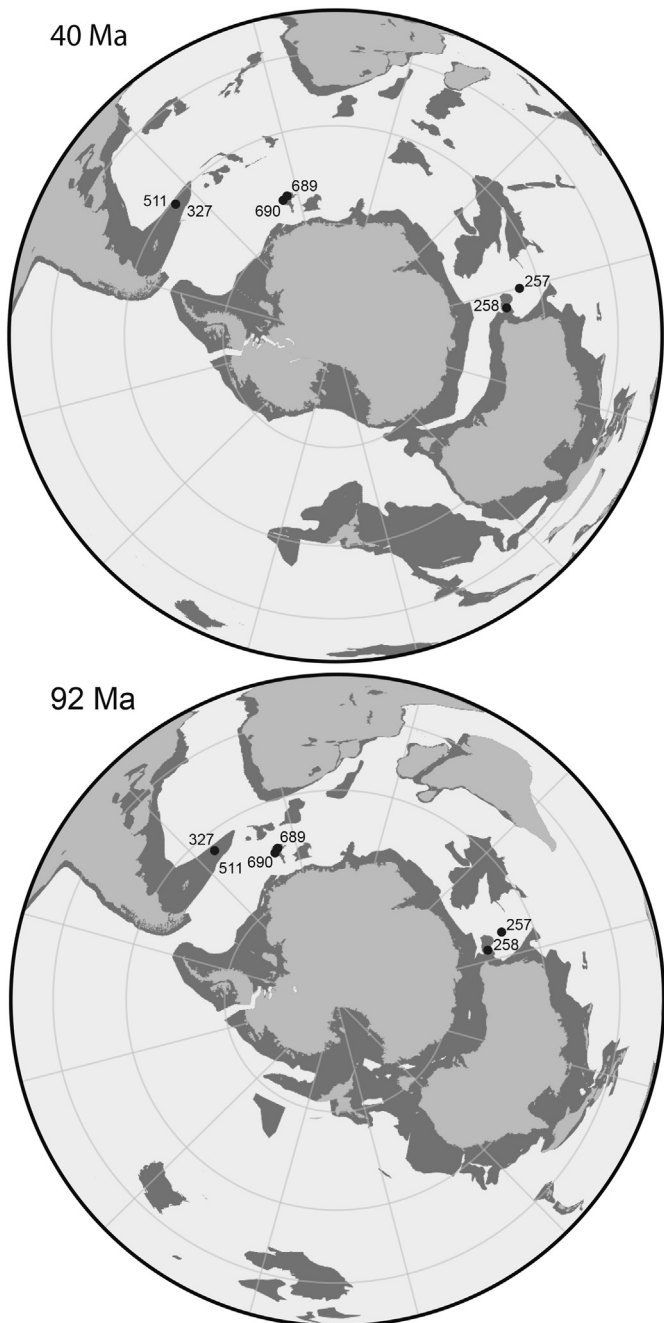
Fig. 1. Paleogeographic reconstructions for the earliest Turonian (94 Ma) and late Eocene (40 Ma) showing location of deep-sea sites discussed in the text. Reconstructions based on Müller et al. (2016).

impossible as the modeled ^{18}O-depleted seawater was too brackish for the diverse, open ocean microfossil assemblages present. Foraminiferal preservation in the Turonian at Site 511 is excellent arguing against diagenetic overprints of > 2‰ that are required to match even 2500 ppmv CO$_2$ models.

In spite of widespread evidence for extreme global warmth during the Cenomanian–Turonian, some authors have argued for the episodic existence of continental ice based on presumed isochrony of sequence stratigraphic boundaries and correlation with oxygen isotope shifts (Gale et al., 2002; Miller et al., 2003, 2005; Stoll and Schrag, 2000; Bornemann et al., 2008). The proposed ice sheet events during the Cretaceous hot greenhouse have been countered by more recent studies that showed oxygen isotopic records are inconsistent with waxing and

waning of continental ice sheets at these times (Ando et al., 2009; MacLeod et al., 2013; Moriya et al., 2007). Significant uncertainty in the timing and extent of sea level falls and the influence of dynamic topography on local tectonics and regional climatic conditions have further weakened support for ice volume variation as a global forcing mechanism for sea level change during the mid-Cretaceous (Haq and Huber, 2017). While an ice-free Turonian now seems widely accepted, the existence of ephemeral ice sheets during cool greenhouse intervals of the Aptian–Albian and Maastrichtian continues to be debated (Alley and Frakes, 2003; Bowman et al., 2013, 2014).

High latitudes respond more strongly than low latitudes to climate forcing, and the Cretaceous southern high latitudes (SHL) are critical in examining disagreements among studies (e.g., large differences between model and proxy temperature estimates exemplified by the Site 511 data, apparent contradictions between inferred glacio-eustatic sealevel changes and lack of glacial evidence in cores recovered around Antarctica). To test proposed patterns and improve knowledge of temperature evolution at SHL, we have compiled published high latitude carbon and oxygen isotopic data from foraminifera with very good to excellent preservation and generated new data to augment and expand existing records. All data are plotted using age models revised herein to facilitate comparisons with CO_2, volcanism, tectonism, and proxies for Cretaceous atmospheric CO_2 composition.

Our new compilation spans 80 m.y. of subpolar history and shows similar oxygen isotopic trends among multiple benthic and planktonic foraminifer species that reflect changes in Earth's sea surface temperatures (SSTs) and sea floor temperatures across the rise and fall of the Cretaceous hot greenhouse climate between 58° and 65 °S paleolatitude. Comparison of maximum and minimum Cretaceous temperatures with those of the Paleogene provides a context for identifying times during the Cretaceous when the existence of polar ice sheets were most likely. Incorporation of recent estimates of volcanic activity, tectonism, and pCO_2 history into our compilation allows assessment of relationships between estimated temperatures and these potential controlling variables and illuminates areas where better constrained data are needed to advance understanding.

2. Methods and studied sections

New data presented in this study were obtained from single species separates of well-preserved planktonic and benthic foraminifera picked from DSDP Sites 257, 258 and 511. Stable isotope results are reported in δ-notation on the Vienna Pee Dee Belemnite (VPDB) scale. Samples analyzed were picked from washed residues. Analyses used 1–30+ individuals for each measurement targeting sample weights of between 50 and 100 μg. Measurements were made on a Kiel III carbonate device linked to a Delta Plus isotope ratio mass spectrometer. Analytical precision is < 0.03‰ and 0.06‰ (1 s.d.) for $\delta^{13}C$ and $\delta^{18}O$, respectively, based on long term tracking of uncorrected results for NBS-19. One split of NBS-19 is run every 7 to 8 samples, and day-to-day variability is corrected for by adjusting results for that day by the difference between the average value of NBS-19 samples measured within that run and nominal values of 1.95‰ for $\delta^{13}C$ and −2.20‰ $\delta^{18}O$. Planktonic and benthic paleotemperatures were calculated from $\delta^{18}O$ values using the equation of Kim and O'Neil (1997) reformulated for synthetic calcite by (Bemis et al. (1998) assuming a $\delta^{18}O_{sw}$ value of −1.27‰ Vienna standard mean ocean water (VSMOW) for Cretaceous seawater in a non-glacial world (Shackleton and Kennett, 1975) adjusted by 0.27‰ to accurately combine input values on the VPDB and VSMOW scales for calcite and seawater, respectively. The temperature estimates have not been adjusted for possible regional variations in $\delta^{18}O_{sw}$, but assumptions regarding $\delta^{18}O_{sw}$ are explored in Section 4.1 below. See Pearson (2012) for thorough discussion of assumptions about $\delta^{18}O_{sw}$ in an assumed ice-free world, planktonic foraminiferal vital effects, inter-individual planktonic foraminiferal variability in $\delta^{18}O$, and variability in individual depth habitats.

Below is a summary of the geologic setting, age control, and foraminiferal preservation for each of these deep-sea sites. The primary resource for the planktonic foraminiferal taxonomy used in this study is from the "pforams@mikrotax" database (http://www.mikrotax.org/pforams/index.html; Huber et al., 2016). Calcareous nannofossil age assignments follow the CC scheme of (Perch-Nielsen, 1985). A more thorough biostratigraphic and taxonomic treatment of Sites 257 and 258 will be presented in a separate work. Ages used for the age models are based on the 2016 Geologic Time Scale (Ogg et al., 2016) and a 2017 data extract from TimeScale Creator 2017 (https://engineering.purdue.edu/Stratigraphy/tscreator/index/index.php).

2.1. Southern Indian Ocean, Wharton Basin: DSDP Site 257

At DSDP Site 257, Albian claystone yielding extraordinarily well preserved calcareous plankton was recovered in an interval from 199.7 to 248.9 mbsf. The base of this interval is 9.2 m above the basaltic basement. The site was drilled in 5278 m water depth and is located in the Perth Abyssal Plain in the southeastern Wharton Basin (30°59.16′S, 108°20.99′E, SE Indian Ocean; Davies et al., 1974). The paleolatitude of the site was ~62°S at 110 Ma according to the plate tectonic reconstruction of Müller et al. (2016) and the Albian sequence was probably deposited at a bathyal paleodepth (Davies et al., 1974).

2.1.1. Biostratigraphy

In most samples analyzed from cores 257–8 and −9 foraminiferal abundance relative to sediment volume is low and planktonic foraminifera are less common (typically < 15% of the population) than benthic foraminifera. The preservation of the calcareous tests, though, is good to excellent (Table 1). Most shells show no infilling and have translucent (glassy) walls with no evidence of secondary shell alteration (see images in Fig. 2). An early Albian age is assigned to cores from 257-7-CC to -9-2, 40–42 cm based on identification of *Microhedbergella praeplanispira*, *M. renilaevis* and *M. rischi*. This assemblage is correlated with the *Ticinella madecassiana* Zone, which spans from 112.4 to 111.8 Ma (Ogg et al., 2016). Planktonic foraminifera are absent from Sample 257-9-2, 110–112 cm.

The interval from Sample 257–8-1, 92–94 cm through 257–9-1, 130–132 cm contains abundant to common, moderately-preserved calcareous nannofossils. The assemblages include few specimens of *Prediscosphaera columnata* with coccolith diameters < 5 μm as well as rare *Hayesites albiensis*. There are no specimens of *Cribrosphaerella ehrenbergii* or *Tranolithus orionatus*. This association indicates the sample comes from the lower, but not the lowest, portion of Subzone CC8a (=Subzone NC8b) of early Albian age. Specifically, this interval is correlated by (Gradstein et al., 2016) to an age of 111.3–112.65 Ma, with a mean age of 112.0 Ma ± 0.7 Ma uncertainty. The common presence of *Seribiscutum primitivum* indicates a high-latitude (austral) affinity for the surface waters at this site and it corroborates the age placement. As reported by Thierstein (1974) in his initial examination of this interval, samples below Section 257-9-1 exhibit increasingly poor preservation, and in the oldest samples only robust species are present and identifiable.

2.1.2. Stable isotope data

We measured stable isotopic values of two benthic and one planktonic species from six sample levels between 238.42 and 248.90 mbsf at Site 257 in sediments assigned to the upper lower Albian (Table 2; Fig. 3). Insufficient numbers of individuals of planktonic foraminifera were present in samples below 240.22 mbsf to analyze accurately.

2.2. Southern Indian Ocean, Mentelle Basin: DSDP Sites 258, 258A

A 525 m sequence of marine sediments was discontinuously cored at DSDP Site 258 (33°47.69′S, 112°28.42′E) in the western Mentelle Basin, which borders Naturaliste Plateau to the west (Davies et al., 1974).

Table 1

Distribution of Albian foraminifera at DSDP Site 257. Preservation ratings are: E = excellent (glassy shell wall), G = good (frosty shell walls but no shell infilling), and M = moderate (significant shell recrystallization and/or shell infilling). Abundance ratings are: C = common, F = few, R = rare. Samples where "x" is shown in place of relative abundance values denote presence of the species.

Site 257	Depth	Age	P. F. Zone	Preservation	Total Foram Abundance	% Planktics	Mi. renilaevis	Mi. praeplanispira	Mi. rischi	Muricohedbergella sp.	Ticinella cf. madecassiana
7, CC	207.08	m. Albian	T. madecassiana	G	C	–	x	x	x	x	x
8-1, 92–94	238.42	m. Albian	T. madecassiana	E	C	4%	9	12	4	x	
8-1, 134–136	238.84	m. Albian	T. madecassiana	E	C	52%	49	35	22		2
8-2, 58–60	239.58	m. Albian	T. madecassiana	E	C	1%					
8-2, 122–124	240.22	m. Albian	T. madecassiana	E	C	6%	2	2	1		2
9-1, 105–109	248.05	m. Albian	T. madecassiana	G	C	–	x	x	x		x
9-1, 130–132	248.30	m. Albian	T. madecassiana	E	F	12%	10	7	3		
9-2, 40–42	248.90	m. Albian	T. madecassiana	E	R	14%	11	6	2		1
9-2, 110–112	249.60	?	?	G	R	0%					
10-1, 110–112	257.60	?	?	M	R	0%					

According to plate reconstructions by Müller et al. (2016) this site was located at about 62°S during the mid-Cretaceous (Fig. 1). The upper 114 m of the cored interval was assigned to the upper Miocene–Recent and the underlying 411 m was assigned to the mid- to Late Cretaceous. The sequence was spot-cored with about ~50% recovery, such that in total only 22% was recovered (Fig. 3). A second hole, Hole 258A, was drilled to 123.5 meters below seafloor (mbsf) with the goal of improving recovery of the upper portion of the sequence. Cretaceous sediments discussed in this study consist of nannofossil ooze (258A-8 through -9), nannofossil chalk (cores 258-5 through -13) and organic-rich claystone (258-14) with a distinctive black shale bed at 258-14-1, 47–57 cm.

2.2.1. Biostratigraphy

Foraminifera are abundant and show frosty preservation (presence of micron scale overgrowths) in the ooze and chalk cores from cores 8-9 at Hole 258A and cores 5-10 at Site 258 (Fig. 2a–b). Most samples from Cores 258-11, -12, and -13 are weakly indurated and yield foraminifera that are both strongly recrystallized and infilled with sparry calcite. Claystone samples from Section 258-14-1 yield well-preserved foraminifera, some of which show glassy preservation (shells translucent with no infilling or overgrowths) (Fig. 2c–d). The low abundance of benthic foraminifera (generally < 3%) and the dominance in the benthic assemblage of gavelinellid and gyroidinoidid species suggest that deposition occurred at a middle bathyal depth.

As observed in Herb (1974), biostratigraphic subdivision of the Cretaceous sequence at Holes 258 and 258A is hampered by the low diversity of the planktonic foraminiferal assemblage and absence of standard tropical-subtropical zonal marker species. Nonetheless, several observations in the present study provide helpful constraints on the age of the sequence and have led us to revise the original chronostratigraphic framework for the holes. Revisions include assignment of:

(1) Cores 258A-8 through -9 to the early Campanian *Globotruncanita elevata* Zone (previously unzoned but assigned to the Santonian) based on the presence of *Globotruncana neotricarinata* (Petrizzo et al., 2011), which first occurs in Sample 258A-9-4, 91–94 (119.91 mbsf)

(2) Cores 258-5 through -9 to the Coniacian- Santonian *Dicarinella marginata* Zone (= *Marginotruncana marginata* Zone sensu (Petrizzo, 2001) based on the presence of the nominate taxon, several species of *Marginotruncana*, and the large biserial species *Planoheterohelix reussi* (previously unzoned but assigned to the Coniacian)

(3) Cores 258-11 through -14 to the Turonian *Whiteinella baltica* Zone (sensu (Huber, 1992) based on the presence of the nominate species, *Dicarinella hagni*, *Praeglobotruncana stephani*, and *Whiteinella aprica* (previously unzoned but assigned to the Cenomanian)

The calcareous nannofossil biostratigraphy from Site 258 was originally documented by Thierstein (1974) using a set of informal zones that were not subsequently adopted by others. The site was re-examined two decades later as part of an early attempt to derive an Austral Upper Cretaceous zonation (Watkins et al., 1996). Those data provide means to assign the Site 258 material to the CC Zonation as follows:

1) Sections 5.1 to 5.2: Santonian (Zone CC16) based on the presence of *Eprolithus floralis* and *Lithastrinus grillii* without *Lithastrinus septenarius*

2) Section 5.3 to sample 9-1, 40 cm: middle to upper Coniacian (Zone CC15) based on co-occurrence of *Lithastrinus septenarius* and *Reinhardtites anthophorus*

3) Sample 9-1, 140 cm to -11-1, 90 cm: upper Turonian to lower Coniacian (Zone CC13) based on the presence of *Marthasterites furcatus* without *Micula staurophora*, an association that is characteristic of the upper Turonian (the co-occurrence of the observed FAD of *Micula staurophora* and *Reinhardtites anthophorus* in Sample 9-1,
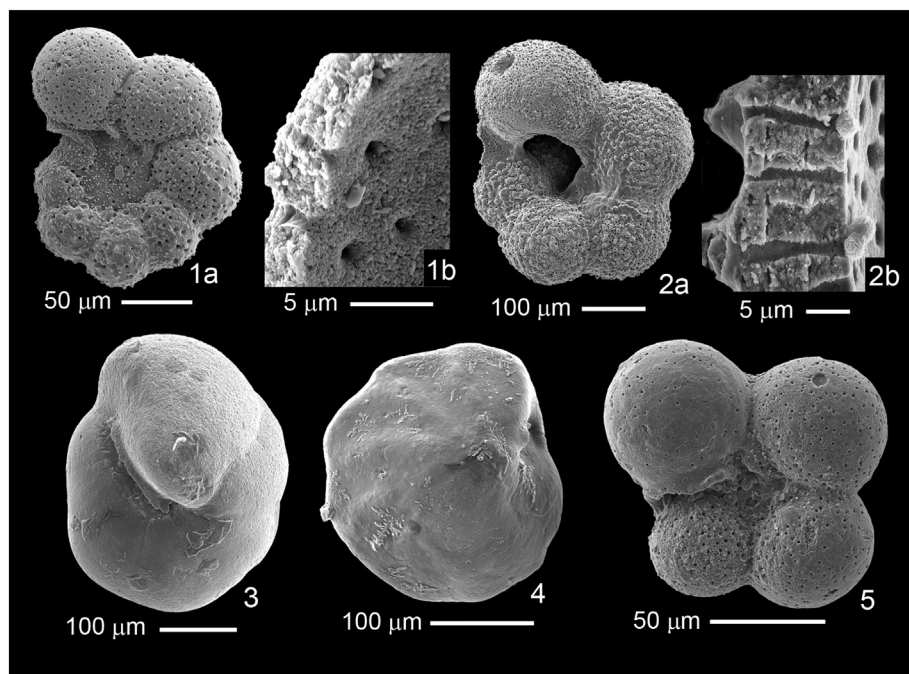
Fig. 2. Preservation of planktonic foraminifera from DSDP Sites 258 and 257. (1a, b) Santonian specimen of *Globigerinelloides bollii* from Sample 258A-5-1,103-106 cm showing minor shell recrystallization in broken section of shell wall; (2a, b) early Turonian specimen of *Whiteinella brittonensis* from uppermost Cenomanian Sample 258-14-1,126-129 cm showing pristine preservation in broken section of shell wall; (3) *Gyroidinoides globosus* from lower Albian Sample 257-9-1, 130–132 cm; (4) *Osangularia schloenbachi* from lower Albian Sample 257-9-1, 130–132 cm; (5) *Microhedbergella renilaevis* from lower Albian Sample 257-8-1, 134–136 cm.

39–40 cm means Zone CC14 is not identified in this sequence)

4) Sample 11-2, 40 cm to 12-3, 40 cm: middle to late Turonian (Zone CC12) based on the presence of *Eiffellithus eximius* without *Marthasterites furcatus*

5) Sample 12-3, 140 cm to 13-4, 70 cm: lower Turonian (Zone CC11) based on the presence of *Quadrum gartnerii* and *Eprolithus moratus* and the absence of *Eiffellithus eximius*

6) Core 14: uppermost Cenomanian (Subzone CC10a) based on the presence of *Lithraphidites acutus*, *Axopodorhabdus biramiculatus* (= *A. albianus* of some authors), and *Helenea chiastia*. The black shale within this core correlates biostratigraphically with OAE 2.

Samples from the base of Section 258A-8-6 and Core 258A-9 contain abundant, well-preserved calcareous nannofossils including *Arkhangelskiella cymbiformis*, *Marthasterites furcatus*, *Lithastrinus grillii*, and *Reinharditites biperforatus*. This assemblage, in the absence of *Broinsonia parca parca* and *B. parca constricta,* indicates the middle to upper part of Zone CC17 of earliest Campanian age. The presence of abundant *Kamptnerius magnificus*, common *Seribiscutum primitivum*, and frequent *Biscutum dissimilis* implies a strongly austral high-latitude affinity for these assemblages.

Ages and depths of calcareous nannofossil and planktonic foraminiferal datum events identified at Holes 258 and 258A are presented in Table 3 and Figs. 4, 6 and 7.

2.2.2. Stable isotope data

We measured stable isotopic values of five benthic and eight planktonic species from 19 sample levels between 124.53 and 264.26 mbsf at Holes 258 and 258A in sediments ranging from the middle Cenomanian-Santonian age (Tables 4, 5; Fig. 3). Previously published $\delta^{13}C$ and $\delta^{18}O$ data from Site 258 from Huber et al. (1995) are also presented. Species belonging to the same genus or family group were combined to maximize stratigraphic continuity of the data plots.

2.3. Southern South Atlantic, Falkland Plateau: DSDP Site 327, Hole 327A

DSDP Site 327 was drilled on the Falkland Plateau Basin (50°52′S, 46°47′W), in 2410 m water depth. The upper Campanian–lower Maastrichtian interval included in this study was spot-cored between 90 and 140 mbsf with < 50% core recovery. Cores 327A-10 through −13 yielded calcareous marl with abundant, well preserved foraminiferal assemblages that are dominated by (> 90%) planktonic foraminifera.

Table 2

Oxygen and carbon isotope measurements from DSDP Site 257 foraminifera. Benthic species include *Gyroidinoides globosus* and *Osangularia schloenbachi*; mixed planktonic samples all belong to the genus *Microhedbergella*.

| Site 257	Depth	*Gyroid. globosus*		*Os. schloenbachi*		*Microhedberg.* spp.	
	(mbsf)	$\delta^{13}C$	$\delta^{18}O$	$\delta^{13}C$	$\delta^{18}O$	$\delta^{13}C$	$\delta^{18}O$
8-1, 92–94 cm	238.42	1.89	−0.53	1.75	−0.33	3.01	−1.46
8-1, 92–94 cm	238.42	1.76	−0.37	1.84	−0.28		
8-1, 134–136 cm	238.84	1.63	−0.60	1.78	−0.34	3.12	−1.62
8-1, 134–136 cm	238.84	1.71	−0.51			2.92	−1.60
8-2, 58–60 cm	239.58	1.74	−0.69	1.99	−0.53		
8-2, 122–124 cm	240.22	1.70	−1.27	1.62	−0.74	3.08	−1.89
8-2, 122–124 cm	240.22	1.59	−1.14	1.49	−0.55	3.09	−1.80
8-2, 122–124 cm	240.22	1.92	−1.18				
9-1, 130–132 cm	248.30	1.65	−0.68	1.64	−0.64		
9-2, 40 cm	248.90	1.93	−0.44	1.85	−0.57		
	Average	1.75	−0.74	1.75	−0.50	3.05	−1.67
	Std. Dev.	0.12	0.33	0.16	0.16	0.08	0.17
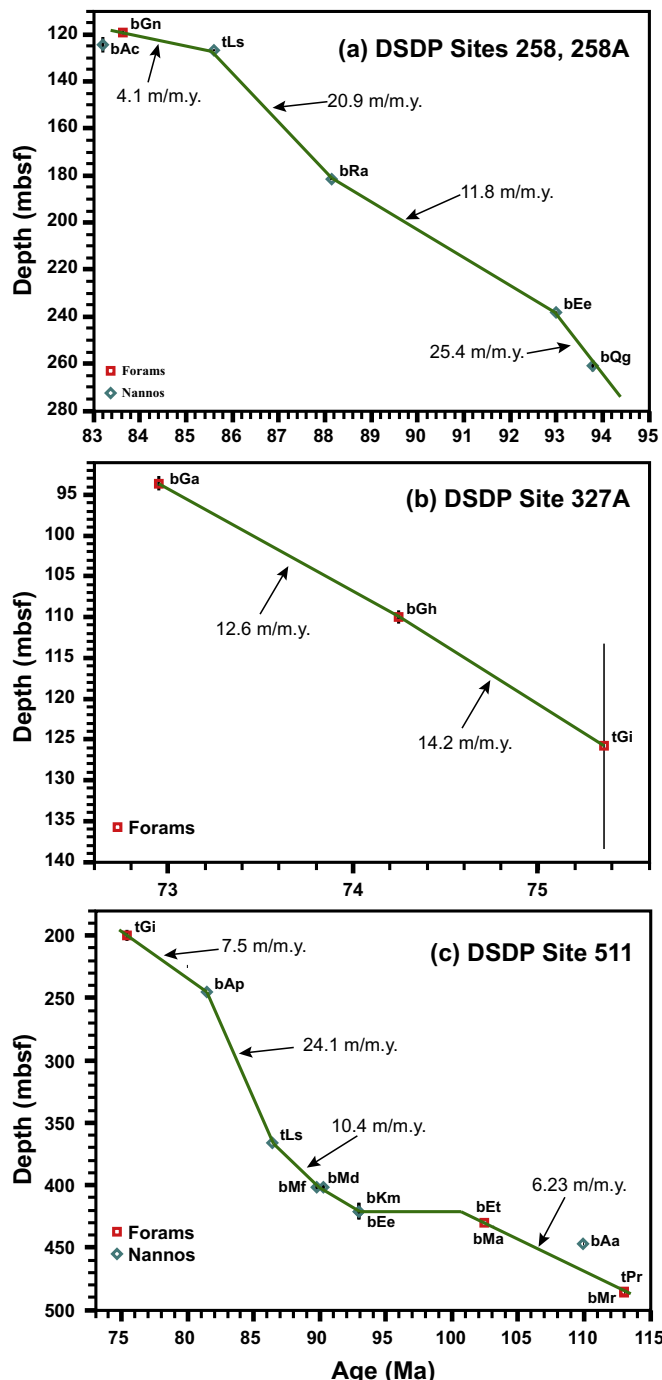
Fig. 3. Age-depth models showing changes in sedimentation rates at DSDP Sites 258 and 258A on Mentelle Basin and DSDP Sites 327A and 511 on Falkland Plateau. Datum abbreviations are listed in Tables 3, 6, 7 and 10.

2.3.1. Biostratigraphy

The planktonic foraminiferal biostratigraphy of the site was discussed in Huber et al. (1995) and is revised in the present study based on additional observations of planktonic foraminifera (datum events listed in Table 6) that were used to construct a new age model from which we estimate sedimentation rates for that 50 m interval (Fig. 4).

2.3.2. Stable isotope data

Previously published Hole 327A $\delta^{13}C$ and $\delta^{18}O$ data from Huber et al. (1995) are presented in Figs. 6 and 7.

Table 3

Ages and depths for planktonic foraminiferal (F) and calcareous nannofossil (N) species from DSDP Sites 258 and 258A used to define the line of correlation in Fig. 4a. Genus spellings are provided in the text. Plot code refers to genus-species abbreviations; FAD = first appearance datum.

Group	Event	Plot code	Age (m.y.)	Top depth (mbsf)	Bottom depth (mbsf)
N	FAD *A. cymbiformis*	bAc	83.20	120.94	127.58
F	FAD *G. neotricarinata*	bGn	83.64	118.30	119.95
N	LAD *L. septenarius*	tLs	85.60	126.39	127.39
N	FAD *R. anthophorus*	bRa	88.14	180.89	181.89
N	FAD *E. eximius*	bEe	92.99	237.91	238.91
N	FAD *Q. gartneri*	bQg	93.80	258.71	263.19
N	FAD *L. acutus/ alatus*	bLa	96.16	264.19	264.19
N	FAD *H. chiastia*	bHc	93.90	264.19	264.19

2.4. Southern South Atlantic, Falkland Plateau: DSDP Site 511

DSDP Site 511 is located in the Falkland Plateau Basin at 51°00′S and 47°58′W at a water depth of 2589 m, about 10 km southeast of DSDP Site 327. Paleogeographic reconstructions indicate that this site was at ~61°S during the early Albian and migrated to ~56°S by the end of the Campanian (Fig. 1). Core recovery, lithologic descriptions, magnetostratigraphy, and initial biostratigraphic interpretations for this site are presented in Ludwig et al. (1983). The upper Aptian-lower Maastrichtian sediments in the present study were cored between 195 and 499 mbsf (cores 23–56) with an average core recovery of 70%. Material at Site 511 was deposited at outer shelf to upper slopes depths during the late Aptian and deepened to middle bathyal depths by the late Albian (Basov and Krasheninnikov, 1983). Lithologies include muddy nannofossil chalk and black shale from 480 to 499 mbsf (cores 55–56), reddish brown muddy nannofossil chalk from 413 to 480 mbsf (cores 48–54), zeolitic claystone from 209 to 412 mbsf, (cores 25–47), and calcareous ooze between 195 and 212 mbsf (cores 23–24). The percent carbonate in the cores is also variable, ranging from 65% in the calcareous ooze to 1% in the zeolitic clay. Dilution by terrigenous clays probably accounts for most of the variability in carbonate content, but shallowing of the foraminiferal lysocline has been proposed to explain loss of the calcareous microfossil record during the late Cenomanian and middle Campanian (Wise Jr, 1983; Basov and Krasheninnikov, 1983).

2.4.1. Biostratigraphy

The more carbonate-rich intervals in the Cretaceous sequence yield abundant foraminiferal assemblages that are dominated by planktonic specimens (usually > 80%), but the claystone sediments yield fewer foraminifera and more variable planktonic:benthic foraminiferal ratios (Huber et al., 1995). Foraminifera show glassy preservation in nearly all samples from the upper Aptian-Campanian interval. In the upper Campanian interval, foraminifera are well preserved but exhibit small-scale shell recrystallization (Krasheninnikov and Basov, 1983; Basov and Krasheninnikov, 1983; Huber et al., 1995; Bice et al., 2003; Fassell and Bralower, 1999).

The planktonic foraminiferal biostratigraphy applied in Huber et al. (1995) and Bice et al. (2003) has been modified in the following ways:

(1) Core 511-23 is reassigned from the lower Maastrichtian to the upper Campanian based on the absence of *Rugotruncana circumnodifer* and *Globotruncana subcircumnodifer*, which are consistently present in Maastrichtian sediments at Maud Rise ODP Sites 689 and 690 (Huber, 1990)

(2) Sections 511-49-5 and -6 are reassigned from the Cenomanian to
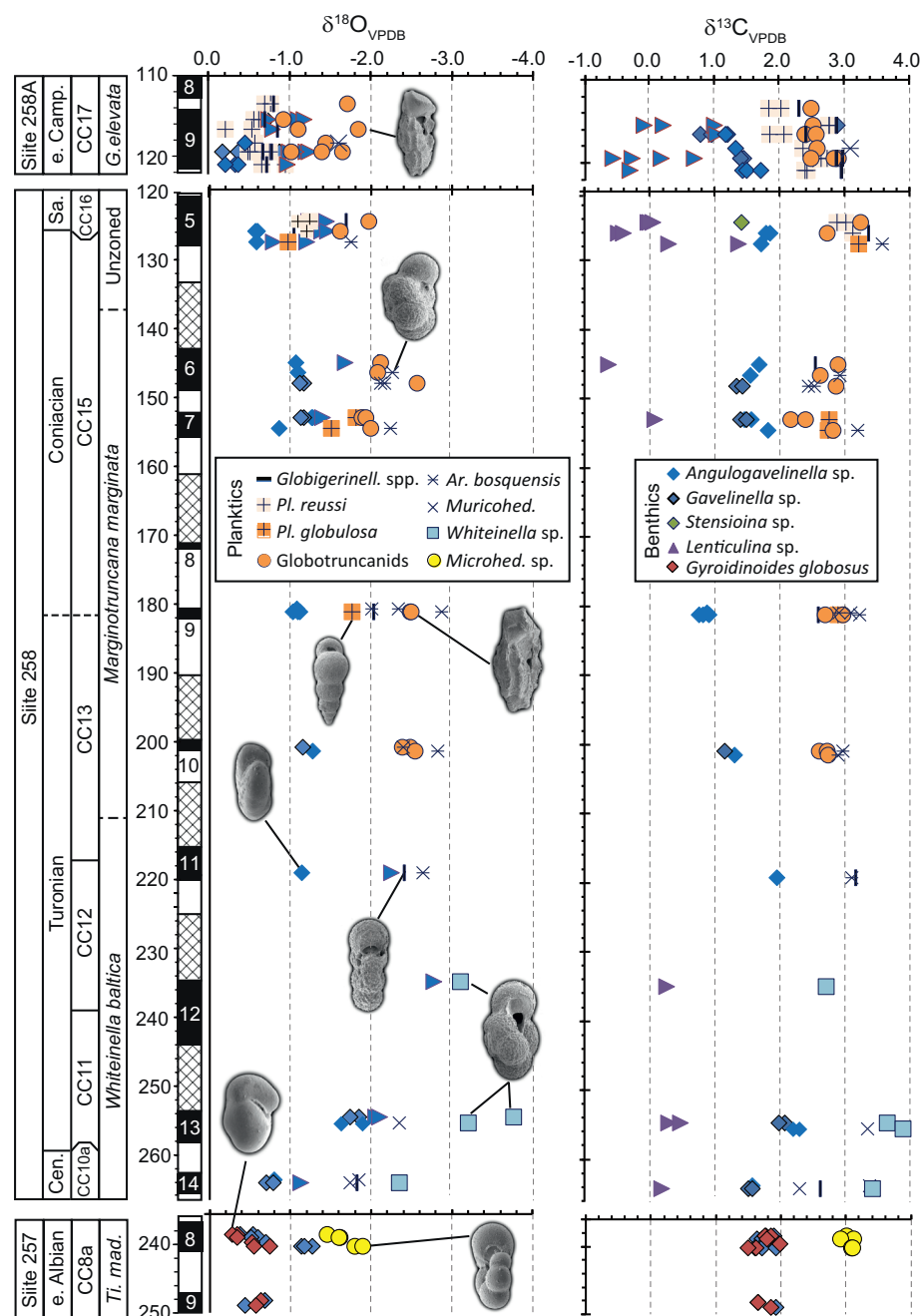
Fig. 4. Oxygen and carbon isotope measurements from planktonic and benthic foraminifera from DSDP Sites 257, 258 and 258A. Columns left to right refer to: DSDP Site, Age, calcareous nannofossil biozone, planktonic foraminiferal biozone, meters below seafloor, and core number. Core fill patterns include black for recovered core, white for un-recovered core, and diamond crosses for uncored intervals. Illustrated specimens on far left are benthics including *Gyroidinoides globosus* and *Gavelinella* cf. *ahuvae*; in middle and right from bottom to top: *Microhedbergella rischi*; *Whiteinella aprica*; *Globigerinelloides yaucoensis*; *Planoheterohelix reussi*; *Globotruncana linneiana*; *Archaeoglobigerina bosquensis*; *Globotruncana neotricarinata*.

the late Albian-early Cenomanian based on the presence of *Muricohedbergella astrepta* and *Pseudothalmaninnella ticinensis*

(3) the Aptian/Albian boundary is placed at 485.46 mbsf (Sample 511-55-4, 60 cm) using the lowest occurrence (LO) of *Microhedbergella renilaevis*, which is the datum now used to define the base of the Albian Stage (Kennedy et al., 2014, 2017). The extinction of several Aptian planktonic foraminifer species, which was the previous criterion for placement of the Aptian/Albian boundary (Huber and Leckie, 2011; Huber et al., 2011), occurs at 486.22 mbsf (511-55-5, 51–52 cm)

Calcareous nannofossils in samples from Sections 511-49-4 through 511-49-6 were investigated to better resolve the previous late Albian-Cenomanian age assignment (Wise, 1983). The samples contain common to few, moderate to poorly-preserved calcareous nannofossils in assemblages dominated by *Watznaueria barnesiae* and *Seribiscutum*

primitivum. The high relative abundance of the latter species indicates the strong austral affinity of samples in this interval precluding direct correlation with low latitude zonal schemes. The presence of (rare) *Gartnerago segmentatum* indicates that the assemblages are no older than early (but not earliest) Cenomanian. Observed *Gartnerago segmentatum* is probably the form reported as *Gartnerago* sp. cf. *G. confossus* by Wise Jr (1983). A maximum early Cenomanian age is corroborated by the presence of *Eiffellithus turrisseifellii* and *Eiffellithus casulus* without their (older) late Albian sister taxa (e.g., *Eiffellithus praestigium*; (Watkins and Bergen, 2003)). Determination of the minimum age is more problematic as it is based on the absence of taxa. The absence of *Quadrum gartneri* and *Kamptnerius magnificus*, which are common components of other austral Turonian assemblages, suggests that this interval is no younger than Cenomanian.

Ages and depths of calcareous nannofossil and planktonic foraminiferal datum events identified at Site 511 are presented in Table 7

Table 4

Oxygen and carbon isotope measurements from DSDP Site 258 foraminifera. Benthic taxa include species of *Angulogavellinella*, *Gavelinella*, *Stensioina*, *Lenticulina*, and *Nuttallides* and the remaining taxa are planktonic species. Genus abbreviations include: *Pl.* = *Planoheterohelix*; *Gt.* = *Globotruncana*; *Ar.* = *Archaeoglobigerina* and *Muricohed.* = *Muricohedbergella*.

Site 258	Depth	Age	Stage	Nanno	Angulogavellinella sp.		Gavelinella sp.		Stensioina sp.		Lenticulina sp.		Nuttallides sp.	
	(mbsf)	(m.y.)		Zone	$\delta^{13}C$	$\delta^{18}O$	$\delta^{13}C$	$\delta^{18}O$	$\delta^{13}C$	$\delta^{18}O$	$\delta^{13}C$	$\delta^{18}O$	$\delta^{13}C$	$\delta^{18}O$
5-1, 103–106	124.53	83.68	Santonian	CC16					1.42	−1.17	0.05	−1.25	1.40	−0.88
5-1, 103–106	124.53	83.68	Santonian	CC16							−0.03	−1.45	1.65	−0.65
5-1, 103–106	124.53	83.68	Santonian	CC16							0.00	−1.23		
5-2, 108–110	126.08	83.80	Santonian	CC16							−0.48	−1.39		
5-2, 108–110	126.08	83.80	Santonian	CC16							−0.41	−1.45		
5-3, 108–111	127.58	83.91	Santonian	CC16							0.28	−1.20		
5-3, 108–111	127.58	83.91	Santonian	CC16							1.37	−0.79		
5-3, 108–111	127.58	83.91	Santonian	CC16										
6-2, 110–113	145.10	85.25	Coniacian	CC15							−0.63	−1.68		
6-3, 110–113	146.60	85.36	Coniacian	CC15										
6-3, 110–113	146.60	85.36	Coniacian	CC15										
6-3, 110–113	146.60	85.36	Coniacian	CC15										
6-4, 110–113	148.10	85.48	Coniacian	CC15			1.34	−1.16						
6-4, 110–113	148.10	85.48	Coniacian	CC15			1.42	−1.12						
6-5, 112–115	149.62	85.60	Coniacian	CC15										
7-1, 106–109	153.06	85.86	Coniacian	CC15			1.39	−1.16			0.08	−1.40		
7-1, 106–109	153.06	85.86	Coniacian	CC15			1.48	−1.13						
7-2, 110–112	154.60	85.98	Coniacian	CC15										
7-2, 110–112	154.60	85.98	Coniacian	CC15										
7-2, 110–112	154.60	85.98	Coniacian	CC15										
7-2, 110–112	154.60	85.98	Coniacian	CC15										
7-3, 110–113	156.10	86.09	Coniacian	CC15										
9-1, 38–41	180.88	87.99	Coniacian	CC15	0.88	−1.09								
9-1, 38–41	180.88	87.99	Coniacian	CC15										
9-1, 79–82	181.29	88.02	Coniacian	CC13	0.83	−1.10								
9-1, 79–82	181.29	88.02	Coniacian	CC13	0.92	−1.12								
9-1, 79–82	181.29	88.02	Coniacian	CC13	0.77	−1.03								
10-1, 142–145	200.92	89.52	Coniacian	CC13			1.15	−1.15						
10-1, 142–145	200.92	89.52	Coniacian	CC13										
10-2, 53–54	201.53	89.57	Coniacian	CC13										
10-2, 53–54	201.53	89.57	Coniacian	CC13										
10-2, 53–54	201.53	89.57	Coniacian	CC13										
11-3, 76–80	219.26	90.92	Turonian	CC12							−1.08	−2.25		
12R-1, 53–55	235.05	92.13	Turonian	CC12							0.26	−2.77		
13R-1, 116–118	254.68	93.63	Turonian	CC11			2.07	−1.85			0.28	−2.06		
13R-1, 116–118	254.68	93.63	Turonian	CC11			1.98	−1.74			0.47	−2.11		
13–2, 54.5–55.5	255.57	93.70	Turonian	CC11	2.24	−1.62								

Table 4 (continued)

Site 258	Depth (mbsf)	Age (m.y.)	Stage	Nanno Zone	Angulogavelinella sp. δ¹³C	Angulogavelinella sp. δ¹⁸O	Gavelinella sp. δ¹³C	Gavelinella sp. δ¹⁸O	Lenticulina sp. δ¹³C	Lenticulina sp. δ¹⁸O	Nuttallides sp. δ¹³C	Nuttallides sp. δ¹⁸O
13-2, 54.5–55.5	255.57	93.70	Turonian	CC11	2.32	−1.86						
14-1, 83–86	263.83	94.33	Cenomanian	CC10a								
14-1, 83–86	263.83	94.33	Cenomanian	CC10a								
14-1, 126–129	264.26	94.37	Cenomanian	CC10a			1.51	−0.70	0.18	−1.13		
14-1, 126–129	264.26	94.37	Cenomanian	CC10a			1.58	−0.79				

Site 258	Gl. prairiehill. δ¹³C	δ¹⁸O	Globigerinell. sp. δ¹³C	δ¹⁸O	Pl. planata δ¹³C	δ¹⁸O	Pl. globulosa δ¹³C	δ¹⁸O	Gt. linneiana δ¹³C	δ¹⁸O	Ar. bosquensis δ¹³C	δ¹⁸O	Whiteinella spp. δ¹³C	δ¹⁸O	Muricohed. sp. δ¹³C	δ¹⁸O
5-1, 103–106	2.86	−1.68			2.89	−1.24			3.25	−1.97						
5-1, 103–106					3.01	−1.09										
5-1, 103–106																
5-2, 108–110	3.35	−1.03			3.12	−1.20			2.73	−1.62						
5-2, 108–110																
5-3, 108–111							3.22	−0.97	2.90	−2.12	3.58	−1.75				
5-3, 108–111																
5-3, 108–111																
6-2, 110–113	2.53	−2.08														
6-3, 110–113									2.62	−2.08	2.93	−2.26				
6-3, 110–113											2.54	−2.12				
6-3, 110–113																
6-4, 110–113									2.86	−2.57	2.45	−2.17				
6-4, 110–113																
6-5, 112–115																
7-1, 106–109							2.76	−1.81	2.17	−1.89						
7-1, 106–109							2.75	−1.51	2.40	−1.93						
7-2, 110–112									2.82	−1.99	3.2	−2.24				
7-2, 110–112																
7-2, 110–112																
7-2, 110–112																
7-3, 110–113																
7-3, 110–113																
9-1, 38–41											2.91	−2.01				
9-1, 38–41											3.10	−2.33				
9-1, 38–41																
9-1, 79–82	2.58	−2.02					2.89	−1.76	2.97	−2.48	3.23	−2.88				
9-1, 79–82									2.70	−2.49						
9-1, 79–82																
9-1, 79–82																
10-1, 142–145									2.61	−2.48	2.98	−2.40				
10-1, 142–145									2.73	−2.39						
10-2, 53–54									2.74	−2.54	2.89	−2.82				
10-2, 53–54																
10-2, 53–54																
11-3, 76–80			3.15	−2.40							3.10	−2.65				
12R-1, 53–55													2.72	−3.10		
13R-1, 116–118													3.65	−3.76		
13R-1, 116–118																
13-2, 54.5–55.5													3.90	−3.20	3.35	−2.35
13-2, 54.5–55.5																
14-1, 83–86			2.61	−1.81												
14-1, 126–129													3.42	−2.35	3.38	−1.85
14-1, 126–129															2.30	−1.74

Table 5

Oxygen and carbon isotope measurements from DSDP Hole 258A foraminifera. Benthic taxa include species of *Gavelinella*, *Angulogavelinella*, and *Lenticulina* all remaining species are planktonic. See caption of Table 4 for explanation of genus abbreviations.

Site 258A	Depth (mbsf)	Nanno Zone	Stage	*Gavelinella* sp. $\delta^{13}C$	$\delta^{18}O$	*Lenticulina* sp. $\delta^{13}C$	$\delta^{18}O$	*Angulogavelinella* sp. $\delta^{13}C$	$\delta^{18}O$	*Gl. prairiehillensis* $\delta^{13}C$	$\delta^{18}O$	*Pl. planata* $\delta^{13}C$	$\delta^{18}O$	*Gt. linneiana* $\delta^{13}C$	$\delta^{18}O$	*Ar. bosquensis* $\delta^{13}C$	$\delta^{18}O$
8-6, 141–144	113.41	CC17	lwr. Camp.			−2.81	1.12			2.29	−0.79	2.02	−0.77	2.49	−1.72		
8-6, 141–144	113.41	CC17	lwr. Camp.									1.84	−0.69				
9-1, 141–143	115.41	CC17	lwr. Camp.	2.90	−0.72	1.02	−0.75			2.86	−0.68	2.78	−0.57	2.53	−0.92		
9-1, 141–143	115.41	CC17	lwr. Camp.			0.23	−1.11					2.77	−0.62				
9-1, 141–143	115.41	CC17	lwr. Camp.			−0.07	−1.18										
9-2, 105–107	116.55	CC17	lwr. Camp.	0.80	2.30			1.22	2.54			2.08	−0.54	2.41	−1.11		
9-2, 105–107	116.55	CC17	lwr. Camp.	0.97	2.26	1.05	−0.80	1.18	2.29	2.40	−0.84	1.86	−0.21	2.58	−1.85		
9-3, 130–133	118.30	CC17	lwr. Camp.					1.33	−0.46			2.37	−0.57	2.59	−1.45	3.10	−1.61
9-3, 130–133	118.30	CC17	lwr. Camp.														
9-3, 130–133	118.30	CC17	lwr. Camp.														
9-3, 130–133	118.30	CC17	lwr. Camp.														
9-4, 91–94	119.41	CC17	lwr. Camp.	1.41	−0.87	−0.55	−1.21			2.96	−0.66	2.52	−0.68	2.49	−1.02		
9-4, 91–94	119.41	CC17	lwr. Camp.			−0.25	−1.24					2.52	−0.76	2.90	−1.65		
9-5, 95–97	119.45	CC17	lwr. Camp.	1.45	−0.18	0.20	−1.09			2.87	−0.76	2.74	−0.52	2.84	−1.41		
9-5, 95–97	119.45	CC17	lwr. Camp.	1.41	−0.37	0.71	−1.00					2.65	−0.49				
9-6, 94–96	120.94	CC17	lwr. Camp.			−0.28	−0.98	1.45	−0.33	2.94	−0.71						
9-6, 94–96	120.94	CC17	lwr. Camp.					1.51	−0.37			2.40	−0.95				
9-6, 94–96	120.94	CC17	lwr. Camp.					1.72	−0.21			2.43	−0.66				

and estimates of sedimentation rates are shown in Fig. 4. The age model indicates that the stable isotope record covers a range from 113.8 to 74.3 Ma and is interrupted by a 10.4 m.y. hiatus spanning from the late Albian (102.2 Ma) through early Turonian (91.8 Ma).

2.4.2. Stable isotope data

New $\delta^{13}C$ and $\delta^{18}O$ data from Site 511 presented in Table 8 and Fig. 6 were generated mostly from the uppermost Aptian through upper Albian interval. Additional late Aptian-late Campanian data were compiled from several sources (Huber et al., 1995; Fassell and Bralower, 1999; Bice et al., 2003).

2.5. Southern South Atlantic, Maud Rise: ODP Sites 689 and 690

Ocean Drilling Program (ODP) Sites 689 (64°31′S, 03°06′E) and 690 (65°10′S, 1°12′E) were drilled on Maud Rise in the southern South Atlantic at 2080 and 2900 water depth, respectively (Barker and Kennett, 1988). The sites occupied nearly the same latitude during the Late Cretaceous-Paleogene (Müller et al., 2016), and benthic foraminiferal assemblages indicate they were deposited at upper abyssal to lower bathyal paleodepths (Thomas, 1990). Core recovery, lithologic descriptions, magnetostratigraphy, and biostratigraphic interpretations for the sites are presented in Barker and Kennett (1988).

2.5.1. Biostratigraphy

Age models for Sites 689 and 690 (Tables 9, 10; Fig. 5) are primarily based on the high quality magnetostratigraphic records reported in Hamilton (1990) and Spiess (1990) with additional control provided by the level of the Cretaceous/Paleogene boundary and several planktonic foraminiferal datum events recorded by Stott and Kennett (1990). Both records show continuous deposition except for a brief hiatus identified in the upper lower Eocene (Thomas et al., 1990).

2.5.2. Stable isotopes

Oxygen and carbon isotope data from ODP Sites 689 and 690 in Fig. 6 are compiled from Barrera and Huber (1990), Stott and Kennett (1990), Barrera and Savin (1999), Huber et al. (2002), and Friedrich et al. (2006). They are plotted using the revised age models discussed above.

3. Stable isotope results

New stable isotope results from Holes 257, 258, 258A, and 511 are presented in Tables 2, 4, 5, and 8, respectively. Temperature estimates shown parenthetically assume seawater $\delta^{18}O$ of −1‰$_{SMOW}$ and use the paleotemperature equation of (Kim and O'Neil, 1997) reformulated for synthetic calcite by Bemis et al. (1998). The summaries below integrate both new and published data.

3.1. Wharton Basin

In the early Albian samples from Hole 257 (Fig. 3), the $\delta^{18}O$ composition of the two benthic species, *Osangularia schloenbachi* and *Gyroidinoides globosus*, average −0.5‰ (13.5 °C) and −0.8‰ (14.7 °C), respectively, with *G. globosus* $\delta^{18}O$ values showing greater variability. Combined planktonic species of *Microhedbergella rischi* and *M. praeplanispira* yield average $\delta^{18}O$ values of −1.7‰ (~18 °C) and show little variability. The $\delta^{13}C$ analyses of the two benthic species both average 1.8‰, with *G. globosus* showing greater variability than *O. schloenbachi*. The $\delta^{13}C$ values from *Microhedbergella* spp. average 3.1‰ and show little variability. The average vertical (planktonic to benthic) $\delta^{18}O$ gradient for the lower Albian is 0.9 to 1.2‰ (~3.3 to 4.5 °C), and the average vertical $\delta^{13}C$ gradient is 1.3‰.

Table 6

Ages and depths determined for planktonic foraminifera from DSDP Site 327A used to constrain the line of correlation in Fig. 4b. Plot code refers to genus-species abbreviations; FAD = first appearance datum.

Event	Plot code	Core Sample	Top Depth	Bott. Depth	Mean Depth	Datum Age[a]
FAD *Globotruncana arca*	bGa	327A-10-3, 22–30	94.50	92.74	93.62	72.95
FAD *Globtruncanella havanensis*	bGh	327A-12-1, 69–72	110.80	109.20	110.00	74.25
FAD *Globigerinelloides impensus*	tGi	327A-13-1, 143–145	113.20	138.43	125.82	75.36

[a] Mean ages calculated from Maud Rise datum events; see Tables 9, 10

Table 7

Ages and depths for planktonic foraminiferal (F) and calcareous nannofossil (N) species from DSDP Site 511 used to constrain the line of correlation in Fig. 4c. Plot code refers to genus-species abbreviations; FAD = first appearance datum; LAD = last appearance datum.

Group	Event	Plot code	Age	Top depth	Bottom depth	Mean depth
F	FAD *Globigerinelloides impensus*	tGi	75.36	195.38	204.70	200.04
N	FAD *Aspidolithus parcus parcus*	bAp	81.43	245.00	246.50	245.75
N	LAD *Lithastrinus septenarius*	tLs	86.38	366.00	366.00	366.00
N	FAD *Micula furcatus*	bMf	90.24	399.00	404.40	401.70
N	FAD *Micula decussata*	bMd	89.77	399.00	404.40	401.75
N	FAD *Eifellithus eximius*	bEe	92.99	413.90	427.90	420.90
N	FAD *Kamptnerius magnificus*	bKm	92.99	413.90	427.90	420.90
F	FAD *Muricohedbergella astrepta*	bMa	102.43	429.65	430.96	430.31
N	FAD *E. turriseiffeli*	bEt	103.13	434.00	434.00	434.00
F	FAD *Microhedbergella renilaevis*	bMr	113.00	485.11	485.46	485.29
F	LAD *Paraticinella rohri*	tPr	113.00	486.12	486.14	486.13

3.2. Mentelle Basin

Early Turonian-early Campanian foraminifera from DSDP Holes 258 and 258A yield oxygen isotope ratios that suggest warmest temperatures during the early Turonian and coolest temperatures during the early Campanian (Fig. 3). In Core 258-13 benthic foraminiferal values range from −1.7 to −2.0‰ (~18–19 °C), and surface mixed layer planktonic foraminiferal values range from −3.2 to −3.8‰ (25–28 °C). These values are ~1.0‰ lower than the underlying uppermost Cenomanian $\delta^{18}O$ values, which were obtained from just below the inferred OAE 2 black shale bed in Core 14. Benthic and planktonic values are relatively constant from the middle Turonian through late Coniacian and then increase by ~0.5‰ near the Coniacian/Santonian boundary. The highest $\delta^{18}O$ values occur in the lower Campanian at Hole 258A with benthic values near −0.5‰ (~13 °C) and mixed layer planktonics averaging −1.4‰ (~17 °C).

Carbon isotope ratios from planktonic and benthic foraminifera (excluding *Lenticulina*) also show relatively small differences between the highest values in the Turonian and the lowest values in the lower Campanian. *Lenticulina* is not considered for comparison because the highly variable $\delta^{13}C$ are characteristic of the genus perhaps related to an unusually flexible ecology with individuals able to shift from epifaunal to deep infaunal habitats (see Wendler et al., 2013 and references therein). The vertical $\delta^{18}O$ gradient is largest in the Turonian (~1.9‰) and smallest in the early Campanian (< 1.0‰), whereas the vertical $\delta^{13}C$ gradient (excluding *Lenticulina*) shows little change from the Turonian through lower Campanian with differences mostly ranging between 1.0 and 1.8‰.

3.3. Falkland Plateau

Oxygen isotope ratios for planktonic foraminifera from samples at Hole 327A and Site 511 are notable for their remarkably low values of −4.2‰ to −4.7‰ that suggest temperatures of 29–32 °C during the Turonian, as discussed above (Fig. 6). Prior to this interval, a gap spans the entire Cenomanian, and, below that, Albian planktonics exhibit values that are 2–3‰ higher (cooler) than seen in the Turonian samples. Planktonic $\delta^{18}O$ values also increase (cool) following the Turonian warm interval. Maximum $\delta^{18}O$ values of −0.6‰ (13 °C) for surface dwelling species are reached in the late Campanian, the youngest Cretaceous recovered on Falkland Plateau. Benthic taxa show similar patterns but with lower amplitude shifts such that $\delta^{18}O$ values are 0.5‰ in the Albian (8 °C), decrease to −1.9‰ (19 °C) during the Turonian, and then gradually increase back to 0.5‰ (8 °C) from the Coniacian through the Campanian.

Carbon isotope ratios also show a major negative excursion across the Aptian/Albian boundary interval (AABI), with pre-excursion benthic values at 113.8 Ma ranging between 1.4 and 2.2‰, decreasing to minimum values of −3.3‰ at 113.0 Ma, and increasing to between 0.0 and 1.4‰ at 112.8 Ma. The latest Aptian planktonic data from within the excursion interval 30 kyr below the boundary level (113.0 Ma) mostly range from 0‰ to −1.1‰ with minimum and maximum values of −2.2‰ and 1.4‰, respectively. Benthic and planktonic $\delta^{13}C$ values show no obvious trends from the early through the late Albian. Benthic values mostly range between −0.7 and 0.0‰, and planktonic values range between 1.4 and 2.8‰. Above the Cenomanian gap, benthic $\delta^{13}C$ values shift subtly lower whereas planktonic $\delta^{13}C$ values are largely unchanged until a shift to higher values in Santonian and early Campanian samples. During the Campanian, benthic and planktonic values converge with $\delta^{13}C$ values of −0.5‰ and 2‰ in these two groups, respectively, in the youngest samples.

The trends summarized above indicate large changes in surface to seafloor isotopic gradients. A vertical $\delta^{18}O$ and $\delta^{13}C$ gradient is essentially absent within the AABI excursion interval as the extremes of benthic and planktonic values and the wide range of values (particularly benthic) in both isotope systems is remarkable and result in overlap between sea surface and seafloor values. The vertical $\delta^{18}O$ gradient in the Albian sequence mostly ranges from 1.0‰ to 1.5‰; it reaches 3.5‰ during the Turonian and remains high through the early Campanian, and decreases to 1.5‰ in the late Campanian. The vertical $\delta^{13}C$ gradient is also effectively non-existent during the AABI (although

Table 8

Oxygen and carbon isotope measurements from DSDP Site 511 foraminifera. Benthic taxa include species of *Osangularia, Berthelina,* and *Lenticulina,* and the remaining taxa are planktonic species. Genus abbreviations include: *Os.* = *Osangularia*; *Gy.* = *Gyroidinoides, Paraticin.* = *Paraticinella, Hd.* = *Hedbergella, M.* = *Muricohedbergella,* and *Ar.* = *Archaeoglobigerina.*

Age	Os. schoenb.		Gy. globosus		Berthelina sp.		Lenticulina sp.		Paraticin. rohri		Hd. infracretacea		M. praeplanispira		Ar. bosquensis	
	$\delta^{13}C$	$\delta^{18}O$	$\delta^{13}C$	$\delta^{18}O$	$\delta^{13}C$	$\delta^{18}O$	$\delta^{13}C$	$\delta^{18}O$	$\delta^{13}C$	$\delta^{18}O$	$\delta^{13}C$	$\delta^{18}O$	$\delta^{13}C$	$\delta^{18}O$	$\delta^{13}C$	$\delta^{18}O$
86.54															2.58	−1.83
102.82													2.11	−1.12		
102.82													1.93	−0.86		
103.09													1.81	−1.26		
103.72													2.33	−0.68		
103.72													2.35	−0.67		
104.57													2.22	−0.72		
104.74													2.42	−0.84		
107.25													1.62	−0.79		
107.25													1.70	−0.80		
108.88													2.31	−1.27		
110.24													2.46	−0.93		
110.30			1.41	0.05	2.11	0.09	0.26	−0.46					2.18	−0.79		
110.30							1.06	−0.46					2.31	−1.05		
110.54			1.21	−0.13	1.74	−0.16	0.25	−0.70								
110.54			1.20	−0.10	1.72	−0.08	0.47	−0.69								
110.78			1.24	−0.26	1.82	−0.09	0.92	−0.60					2.29	−0.92		
110.99			1.19	−0.19	1.72	0.12	0.76	−0.72					2.20	−1.55		
110.99			0.97	−0.11												
111.17					1.44	0.17										
111.65	2.05	0.42														
111.92					2.58	0.18							3.38	−0.93		
111.92					2.50	0.27							3.30	−1.10		
112.16			1.32	−0.04	1.70	−0.07										
112.16			1.44	−0.02	1.73	−0.01										
112.39							1.65	−0.47					2.96	−1.22		
112.39			1.65	0.17	2.00	0.11	0.63	−0.60					2.69	−1.35		
112.39			1.55	0.09	1.77	0.01	−0.43	−0.83								
112.64													2.68	−0.64		
112.65	1.60	0.13			2.18	0.01	0.15	−0.56								
112.65	1.65	−0.12	1.08	−0.28	1.65	−0.22										
112.65	1.94	0.07	1.07	−0.24												
112.73	0.83	−0.62	1.09	−0.19	1.49	−0.15	−0.09	−0.71								
112.73			1.00	−0.26	1.35	−0.32										
112.85			0.68	−1.54	0.79	−1.69	2.05	−0.42								
112.85			0.71	−1.35	0.79	−1.68	1.31	−0.75								
112.91			−0.79	−2.97			1.85	−0.80								
112.91			−0.94	−3.65			0.32	−1.71								
112.92			−0.55	−3.01			−0.04	−1.97								
112.92			1.22	−0.53			−0.80	−2.26								
112.94			−0.37	−2.75	−0.70	−3.42	−0.42	−2.75								
112.94			0.81	−1.12	−1.52	−4.47	−0.59	−2.97								
113.00					−1.59	−1.40										
113.00					−3.31	−1.92	−5.19	−2.84								
113.01			0.02	−1.04	0.57	−0.93										
113.01			−1.11	−1.69												
113.02			0.38	−0.52	1.72	−0.28										
113.02	0.21	−0.18	0.32	−0.73												
113.02	1.42	−0.59	0.13	−1.13	−1.31	−3.28	−1.40	−2.61	−0.66	−4.68	−1.08	−2.87				
113.02	0.57	−1.48	−1.09	−2.65	0.98	−0.91	−1.25	−2.66	0.13	−3.74	−2.16	−4.61				
113.03	0.16	−2.07			−1.06	−3.83	1.50	−0.46			−1.37	−3.86				
113.03					−1.25	−4.04	1.53	−0.51			−1.06	−3.43				
113.03							−1.72	−4.05								
113.03							0.45	−0.86								
113.05	0.42	−1.79	−1.16	−3.71	0.27	−1.96										
113.06	0.00	−2.36					0.54	−2.06								
113.06	0.21	−2.39					−0.26	−2.17								
113.06			−0.10	−2.29	−0.85	−3.63	−0.56	−2.22								
113.06			−0.68	−2.73												
113.07			−1.23	−3.84	1.33	−1.11										
113.07			−0.19	−2.37												
113.08			−0.19	−2.65					1.31	−2.96						
113.09			1.37	−0.58	−0.62	−3.37	0.20	−2.46	2.52	−3.12						
113.09					−0.94	−3.85	−0.53	−3.03								
113.11									1.84	−2.99						
113.13	−0.11	−2.42	−0.86	−3.27	−1.30	−4.08	−2.79	−4.84								
113.13			−1.58	−4.07	−0.96	−3.66	0.55	−0.77								
113.30									1.28	−3.43						
113.42			−1.79	−4.53	−2.30	−5.17	0.73	−1.29	−1.00	−5.19	−1.72	−5.64				
113.42			−1.10	−3.75			−1.80	−4.29								

(continued on next page)

Table 8 (continued)

Age	Os. schoenb.		Gy. globosus		Berthelina sp.		Lenticulina sp.		Paraticin. rohri		Hd. infracretacea		M. praeplanispira		Ar. bosquensis	
	$\delta^{13}C$	$\delta^{18}O$	$\delta^{13}C$	$\delta^{18}O$	$\delta^{13}C$	$\delta^{18}O$	$\delta^{13}C$	$\delta^{18}O$	$\delta^{13}C$	$\delta^{18}O$	$\delta^{13}C$	$\delta^{18}O$	$\delta^{13}C$	$\delta^{18}O$	$\delta^{13}C$	$\delta^{18}O$
113.54			−1.57	−3.07	−1.23	−3.45	0.36	−1.60			−2.75	−5.37				
113.54			−1.85	−3.40												
113.65			1.04	0.04												
113.76					1.88	0.25	0.58	−0.38								
113.77					1.44	0.18										
113.77			2.13	0.51	2.35	0.38	1.15	−0.17								
113.77			2.16	0.45												

Table 9

Oxygen and carbon isotope measurements from DSDP Site 511 foraminifera.

Group	Event	Plot code	Age	Depth
M	Base Chron 8N-2	bC8n.2n	25.99	75.97
M	Top Chron 9N	bC8r	26.42	79.46
M	Base Chron I0N	bC10n.2n	28.28	91.93
M	Base Chron11N	bC11n.2n	29.97	103.38
M	Base Chron 12N	bC12n	31.03	106.88
M	Base Chron 15R	bC15r	35.71	135.77
M	Base Chron 16N	bC16r	36.97	145.02
M	Base Chron 17N-3	bC17n.3n	38.33	152.73
M	Top Chron 18N	b17r	38.62	153.70
M	Base Chron 19N	bC19n	41.39	163.16
M	Top Chron 20N	bC19r	42.30	165.55
F	FAD *Planomalina australiformis*	bPa	55.50	207.92
F	FAD *Parasubbotina inconstans*	bPi	62.90	229.84
F	FAD *Parasubbotina pseudobulloides*	bPp	65.70	231.89
K/Pg	K/Pg	K/Pg	66.00	233.42
M	C30N/C30R	bC30N	68.20	246.60
M	C30R/C31N	bC30R	68.37	248.08
M	C31N/C31R	bC31N	69.27	252.92
M	C31R/C32N	bC31R	71.45	259.97
M	C32R.2N/C32n.2R	b32R.2N	73.65	272.33
M	32R.2R/C33N	bC32R.2R	74.31	277.32

variability is high), it is up to 1.2‰ during the Albian, increases to 2.5‰ during the middle Turonian, and it diminishes to 0.8‰ in the late Campanian.

3.4. Maud Rise

Upper Campanian-Maastrichtian samples from Maud Rise (Fig. 6) continue the pattern of change seen in Santonian-upper Campanian samples on Falkland Plateau. The Campanian $\delta^{18}O$ measurements from benthic foraminifera for the Maud Rise sites match values from Hole 327A at 0.5‰ (8 °C), and they continue to generally increase through the Maastrichtian to $\delta^{18}O$ values of 0.7 to 1.3‰ (4 to 7 °C) in samples between 68.3 and 66.5 Ma. A brief 1‰ negative shift between 66.5 and 66.2 Ma is followed by a return to higher values just below the Cretaceous/Paleogene boundary. The planktonic $\delta^{18}O$ data from both Maud Rise sites increase from −1‰ (14 °C) in the late Campanian to 0.5‰ (8 °C) between 66.8 and 66.5 Ma and show a short, 1‰ negative excursion between 66.5 Ma and the Cretaceous/Paleogene boundary. Planktonic $\delta^{18}O$ values are ~0.5‰ higher in samples from Site 689 than in correlative Campanian samples from the same species analyzed from Sites 690 and Hole 327A, but there is no obvious difference in values in the mid- to late Maastrichtian from the two Maud Rise sites.

Benthic $\delta^{13}C$ values in the Maud Rise sites increase gradually from −0.5‰ to 1.5‰ whereas planktonic values vary between 2‰ and 3‰. Late Campanian values in both sites match closely values in correlative samples from Falkland Plateau.

Maud Rise trends also continue the pattern of decreasing vertical

Table 10

Ages and depths for planktonic foraminiferal (F) and calcareous nannofossil (N) species and base magnetic polarity chron boundaries from ODP Site 690 used to constrain the line of correlation in Fig. 6b. Plot code refers to genus-species abbreviations; FAD = first appearance datum.

Group	Event	Plot Code	Age	Depth (mbsf)
M	Top Chron 8N	bC7r	24.76	53.25
M	Base Chron 8N	bC8n.2n	25.99	60.11
M	Top Chron 9N	bC8r	26.42	60.99
M	Base Chron 9N	bC9N	27.44	68.48
M	Base Chron11N	bC11n.2n	29.97	73.93
M	C11R-2/C12N	bC11r	30.59	80.76
M	C12N/C12R	bC12n	31.03	84.01
M	Base C12R	b12r	33.16	91.70
M	C16n.2n	bC16n.2n	36.70	95.70
M	Top Chron 17N	bC16r	36.97	96.59
M	bC19n	bC19n	41.39	105.65
M	~ Top Chron 20N	bC19r	42.30	106.27
M	~Top Chron 2IN	bC20r	45.72	118.74
M	Base Chron 21N	bC21n	47.35	123.63
M	bC21r	bC21r	48.57	130.48
M	Base Chron 22N	bC22n	49.34	132.23
M	C23N-2/C23R-2	bC23n.2	51.83	133.18
M	bC23r	bC23r	52.62	137.33
M	C24R-1/C24N-2	bC24n.1r	53.20	144.42
M	Base Chron 24N	bC24n.3n	53.98	154.62
M	Top Chron 25N	bC24r	57.10	185.48
M	C25N/C25R	bC25n	57.66	195.94
M	C25R/C26N	bC25r	58.96	210.20
M	C26N/C26R	bC26n	59.24	213.06
M	C29N/C29R	bC29n	65.69	247.55
K/Pg	K/Pg	K/Pg	66.04	247.81
M	C29R/C30N	bC29R/C30N	66.40	252.28
M	C31N/C31R	bC31N/C31R	69.27	272.25
M	C31R/C32N	bC31R/C32N	71.45	283.39
M	C32.2N/C32n.2N	bC32.2N/C32n.2R	73.65	302.78
M	32R.2R/C33N	b32R.2R/C33N	74.31	308.02

$\delta^{18}O$ and $\delta^{13}C$ gradients seen at Falkland Plateau. Maud Rise gradients are highest during the late Campanian at 1‰ to 1.5‰ for $\delta^{18}O$ and 2.5‰ to 3‰ for $\delta^{13}C$, decrease to a mid-Maastrichtian minimum of ~0‰ for $\delta^{18}O$ and 1.5‰ for $\delta^{13}C$. The $\delta^{18}O$ increases to 0.5‰ in the late Maastrichtian.

4. Subantarctic temperature changes across 80 m.y

An 80 m.y. compilation of benthic and planktonic $\delta^{18}O$ changes for the late Aptian through late Eocene is based on foraminiferal data plotted against the revised age models for all SHL sites (Fig. 7). High latitude Paleogene isotopic trends have been discussed in many well cited studies (e.g., Stott and Kennett, 1990; Kennett and Stott, 1990; Bohaty and Zachos, 2003; Mackensen and Ehrmann, 1992; Stott et al., 1990; Thomas and Shackleton, 1996); we include those data for SHL here to facilitate comparison of the two most recent and arguably best studied greenhouse intervals—the Late Cretaceous and the early
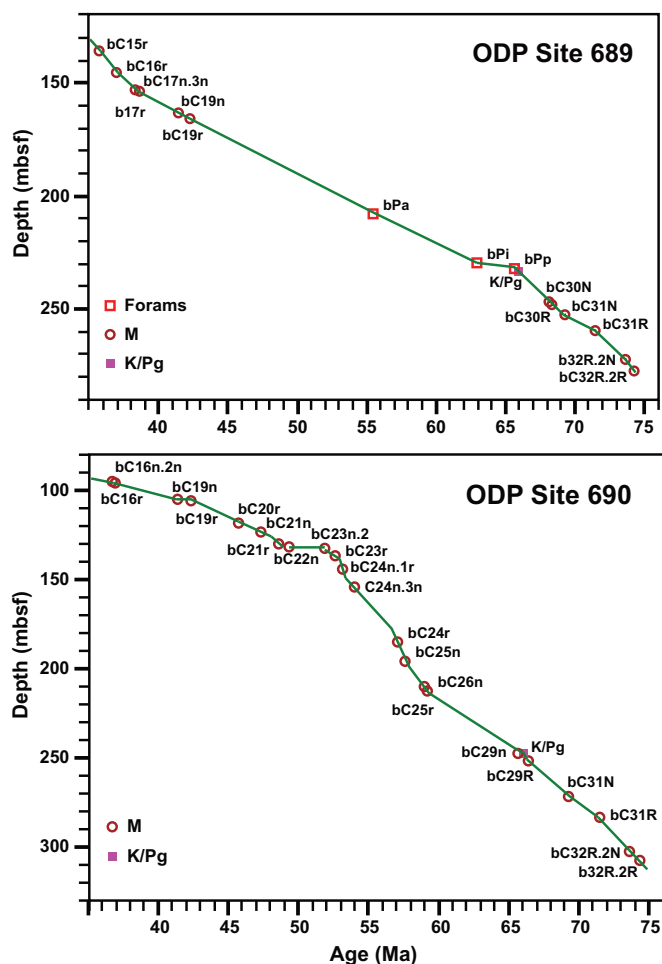
Fig. 5. Age-depth models showing changes in sedimentation rates at ODP Sites 689 and 690 on Maud Rise.

Eocene.

Long-term trends as well as short-term excursions are apparent in the compilation. The most significant oxygen isotope events resolved are the Aptian/Albian boundary interval event (AABI; Huber et al., 2011), Cretaceous Thermal Maximum (KTM), Deccan basaltic province eruption event (Deccan; Barrera and Savin, 1999; Wilf et al., 2003), Paleocene/Eocene Thermal Maximum (PETM; Stott and Kennett, 1990; Kennett and Stott, 1991; Thomas and Shackleton, 1996), and Middle Eocene Climatic Optimum (MECO; e.g., (Bohaty et al., 2009). The extremely low oxygen isotopic values across the KTM and AABI relative to the other events is readily apparent as are generally lower $\delta^{18}O$ during most of the Cretaceous greenhouse interval compared to the Eocene greenhouse. In contrast, values at the transitions are quite comparable. That is, whereas the $\delta^{18}O$ values suggest most of the Cretaceous greenhouse was warmer than its Cenozoic counterpart, apparent SHL temperatures during the Albian, Maastrichtian, and late Eocene are quite comparable. As ice sheets are known to have formed in Antarctica by the late Eocene (e.g., Ehrmann and Mackensen, 1992; Carter et al., 2017), determining whether or not ice was present during the Maastrichtian and Albian would provide two important, additional test cases for the conditions when (and if) glacial ice accumulates and decays, thereby better constraining over what range of conditions the climate system can tip from an ice house to an ice-free state.

4.1. Cretaceous temperatures and δ_w of southern high latitude seawater

New benthic and planktonic foraminiferal $\delta^{18}O$ data from the southern Indian Ocean (Site 258) corroborate low to extremely low $\delta^{18}O$ values previously reported for Falkland Plateau (Sites 511 and 327) and strengthen the argument that the Cretaceous hot greenhouse was warmer than its Cenozoic counterpart. These new data undermine arguments that Falkland Plateau results are anomalous due to local oceanographic and/or sedimentological conditions. Diagenetic artifacts also seem an unlikely explanation for the low values. Excellent preservation at Site 511 is one critical counter argument (Bice et al., 2003). The very good, but frosty, preservation at 258 is a second. During early burial in near seafloor conditions, overgrowths (Fig. 2) would have shifted values toward results for co-occurring benthics and imparted a positive bias in the 258 planktonic results. That is, Turonian planktonic and benthic $\delta^{18}O$ values $< -3.7‰$ and $-1.8‰$, respectively, are observationally well supported based on results from two widely separated sites in which the foraminifera were preserved in different lithologies with different burial histories. If regional seawater had $\delta^{18}O$ values close to the canonical ice-free value of $-1‰_{SMOW}$, $\delta^{18}O$ values of $< -3.7‰$ and $-1.8‰$ imply surface water temperatures $> 27 °C$ and bottom water temperatures $> 19 °C$.

Surface water temperatures in excess of 27 °C at 58–60 °S are problematically warm based on all model results of which we are aware. To achieve ~30 °C surface temperatures during the Turonian, modeling experiments required 6500–7500 ppm CO_2 and a 50% increase in poleward heat transport (Bice et al., 2003). Specific CO_2 levels reported are likely a function of the General Circulation Model used by Bice et al. (2003), as other models with different climate sensitivities and assumed boundary conditions produce different temperature simulations at the same CO_2 levels (e.g., Lunt et al., 2016), but ~30 °C temperatures at 60°S is warm regardless. In a more recent study, at 2800 ppmv CO_2, which is above the upper limit of pCO_2 estimated by paleobarometric proxies for the Late Cretaceous (e.g., Hong and Lee, 2012; Foster et al., 2017; Barral et al., 2017; see Fig. 6), modeled SHL sea surface temperatures are between 10 and 20 °C (Zhou et al., 2012). Sea surface temperatures $< 20 °C$ at 60° paleolatitude are also predicted from latitudinal gradients estimated from Cenomanian and Turonian fish teeth $\delta^{18}O$ values (Pucéat et al., 2007; Martin et al., 2014).

Higher precipitation rates and a steeper trend in the latitudinal gradient in the $\delta^{18}O$ values of precipitation provide a potential resolution to this paradox. Bice et al. (2003) discounted a lowering of seawater $\delta^{18}O$ values through increased runoff and/or a positive precipitation balance to explain Site 511 data as their calculations resulted in predicted salinities that would be too brackish for foraminifera. That study used a $\delta^{18}O$ of $-10‰_{SMOW}$ for freshwater input based on the modern precipitation at comparable latitudes. Using an end member value of $-20‰_{SMOW}$ for precipitation, though, can result in seawater having a $\delta^{18}O$ value of $-3.2‰_{SMOW}$ and salinity of 30 psu (within the range at which modern planktonic foraminifera survive). Foraminiferal tests with a $\delta^{18}O$ value of $-4‰_{V-PDB}$ secreted in equilibrium with $-3.2‰_{SMOW}$ water would have formed at 17.3 °C, still warm for high latitudes, but within the upper range of model predicted temperatures (Fig. 8). An enhanced hydrologic cycle is commonly invoked for greenhouse times, and a positive precipitation balance has been predicted by climate models in the southern South Atlantic during the Turonian (Donnadieu et al., 2016; Zhou et al., 2008). Using predicted salinity and/or predicted $\delta^{18}O$ values of seawater and precipitation inferred from proxy studies (e.g., Huber et al., 2011; MacLeod et al., 2017) relative to model results (Zhou et al., 2008) could be a valuable new validation target in model-data comparisons.

Low salinity surface waters also could explain high surface to seafloor isotopic gradients at SHL that are particularly apparent when SHL trends are compared to long-term trends in other regions (Fig. 9). The Turonian planktonic to benthic $\delta^{18}O$ gradient is as large at SHL as it is in the North Atlantic and larger than in the Indian Ocean. However, if SHL planktonic foraminiferal $\delta^{18}O$ values are low due to both low surface water $\delta^{18}O$ values and warm temperatures whereas surface water $\delta^{18}O$ values contributes little to the planktic to benthic $\delta^{18}O$
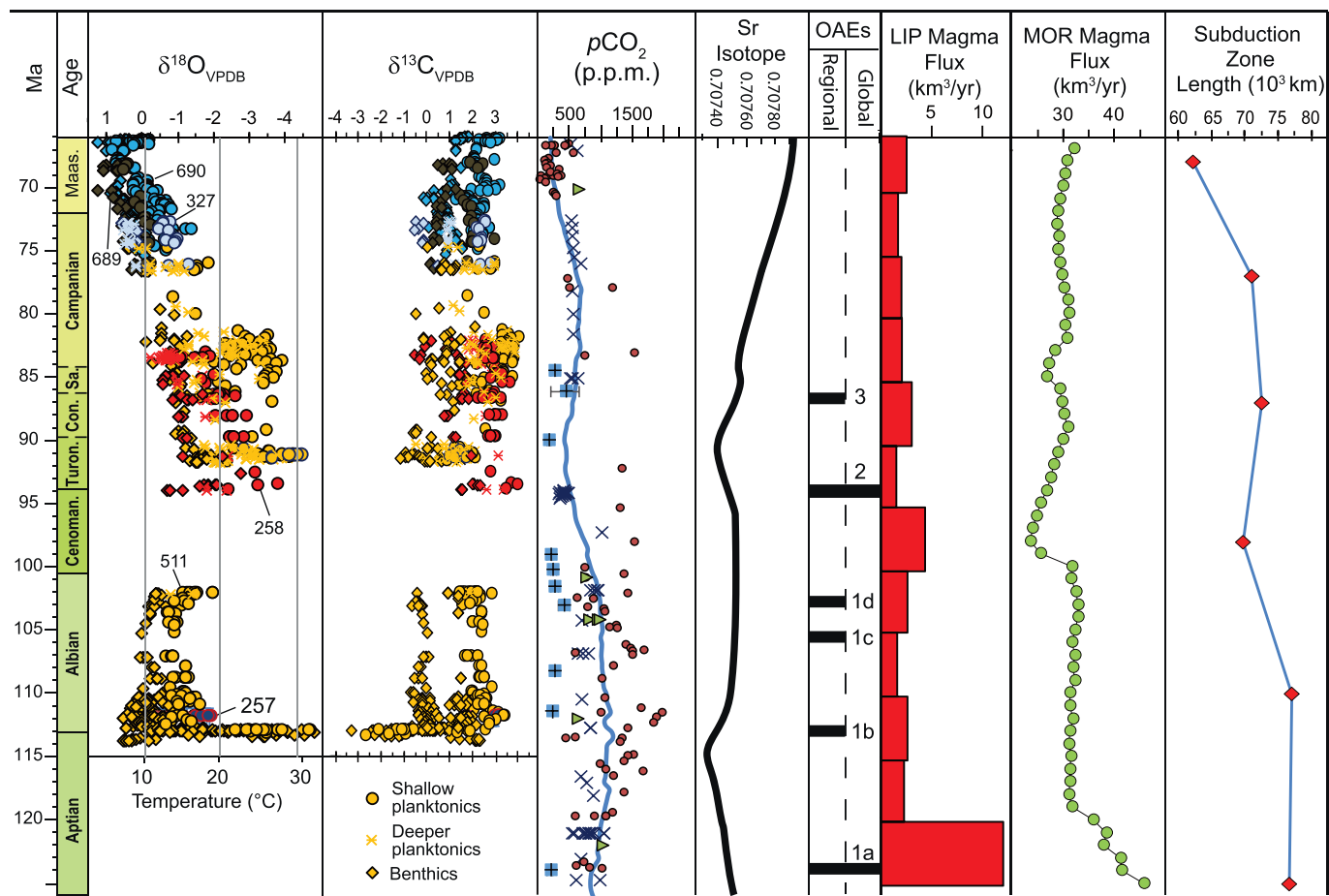
Fig. 6. Compiled Cretaceous oxygen and carbon isotope data for benthic and planktonic foraminifera from Sites 257 and 258 in the southern Indian Ocean and Sites 327, 511, 689 and 690 in the southern South Atlantic (this study) shown relative to (left to right): (1) proxy estimates for Cretaceous pCO_2 including the following: blue squares with crosses: *Frenelopolis* conifer estimates with ± 1σ around the mean pCO_2 level (Barral et al., 2017); green triangles: liverwort $\delta^{13}C$, red circles: pedogenic carbonate $\delta^{13}C$, and crosses: leaf stomata shown with LOESS best fit line through all but conifer data (from Foster et al., 2017 compilation); (2); (3) Sr isotope seawater curve (McArthur et al., 2012); (4) regional and global Oceanic Anoxic Events (Takashima et al., 2006); (5) global large igneous province (LIP) magma flux estimated by Coffin et al. (2006); and (6) global mid-ocean ridge magma flux estimated by Müller et al. (2016). Global subduction zone length estimated by van der Meer et al. (2014). Strongly negative $\delta^{18}O$ and $\delta^{13}C$ values across the Aptian-Albian boundary interval are considered an artifact of a more restricted and shallower depositional basin compared to later periods (see text). (For interpretation of the references to colour in this figure legend, the reader is referred to the web version of this article.)

gradient at other sites, this comparison would be misleading. SHL benthic $\delta^{18}O$ values are generally comparable to values in the North Atlantic, lower than those in the Pacific, and generally higher than those in the Indian Ocean. SHL planktonic to benthic $\delta^{18}O$ gradients decrease markedly after the early Campanian due mainly to a disproportionately large increase in SHL planktonic $\delta^{18}O$ values.

High $\delta^{13}C$ gradients in SHL data are even more dramatic than the high $\delta^{18}O$ gradients. Temporal trends in planktonic and benthic $\delta^{13}C$ values for the three other regions plot almost entirely within the yellow shading bounded by SHL planktonic and benthic $\delta^{13}C$ curves. Planktonic $\delta^{13}C$ values are similar among regions, but SHL benthic $\delta^{13}C$ values are 1‰–2‰ lower than Pacific, North Atlantic, and Indian Ocean benthic values throughout the interval from the Turonian into the late Campanian (Fig. 9). A well stratified water column with limited mixing but with high productivity and efficient organic carbon export from surface waters (that is, an efficient biological pump) would create such a situation.

The success of combined high temperatures and altered hydrology at explaining SHL data for much of the Late Cretaceous notwithstanding, explanations for isotopic patterns across the Aptian/Albian boundary interval (AABI) at Site 511 seem to require incorporation of additional variables. Excess rainfall with low $\delta^{18}O$ values at 20 °C

would result in the low planktonic $\delta^{18}O$ values, but similarly low benthic $\delta^{18}O$ values are puzzling and more difficult to understand because AABI benthic $\delta^{18}O$ values span a 5‰ range. The problem is reversed for $\delta^{13}C$ values where planktonic values span a range of 5‰. Foraminiferal specimens are excellently preserved (glassy) throughout the nearly 9 m thickness of the AABI interval. Further arguing against a diagenetic explanation is that no lithologic break coincides with the transition into or out of the AABI, but lithology varies considerably across the interval with anomalous isotopic values (interbedded black shale and muddy reddish and greenish gray nannofossil chalks). As a working hypothesis, we propose sediments at Site 511 were deposited within a small, shallow, quite restricted and isolated sub-basin at this time. Isolation and a relatively small volume of water within the sub-basin would mean the entire water column might be responsive to changing local conditions. We acknowledge, though, that this is an ad hoc explanation and not an explanationsupported by independent evidence.

4.2. Deepwater circulation

In terms of circulation, the very low benthic $\delta^{13}C$ values indicate SHL bathyal waters were not a significant source for intermediate or
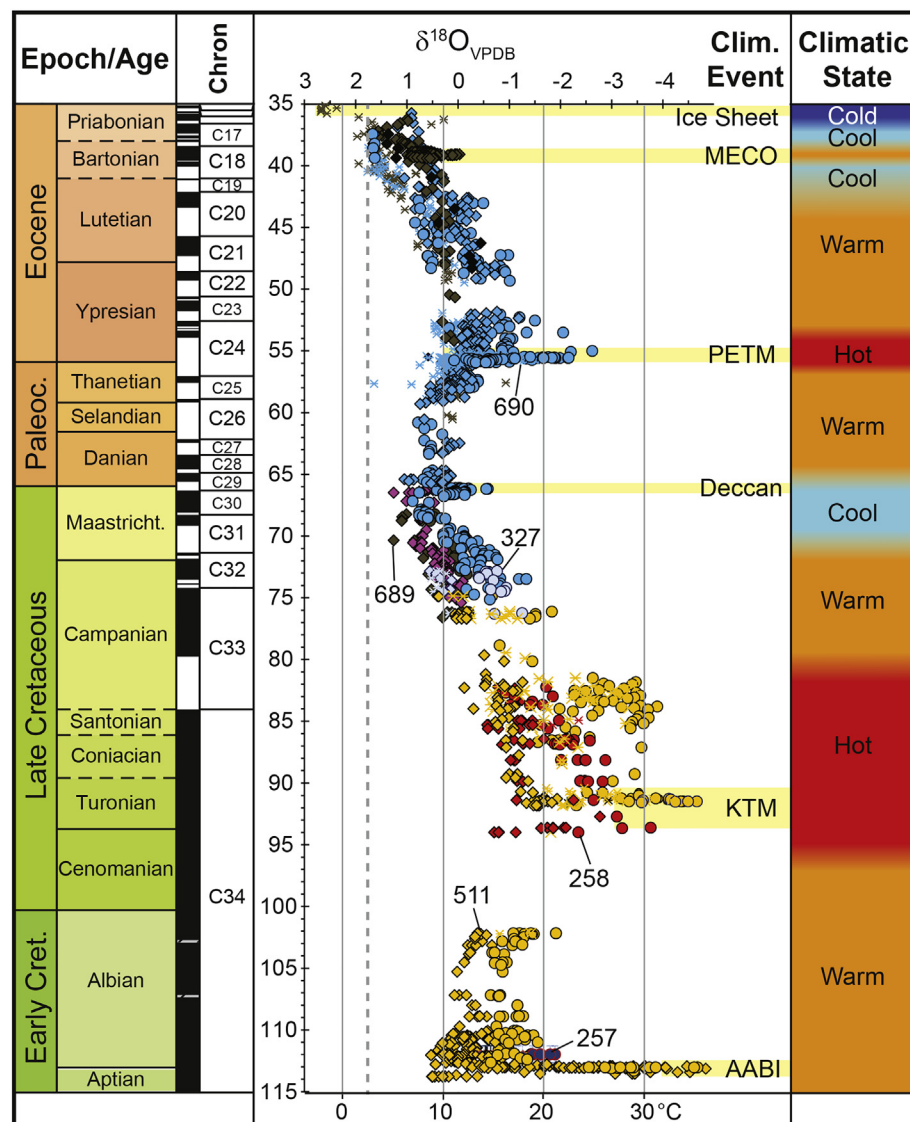
Fig. 7. Cretaceous and Paleogene oxygen isotope data compiled for southern high latitude deep-sea sites, shown relative to changes in global climatic states. Columns are (left to right): (1) geologic age and magnetic reversal chron (exported from TimeScale Creator v. 7.1, https://engineering.purdue.edu/Stratigraphy/tscreator/index/index.php); (2) age; (3) foraminiferal oxygen isotope values for southern high latitude deep-sea drill sites (see Fig. 5 for symbol explanation); (4) climatic events, including AABI = Aptian/Albian Boundary Interval, KTM = Cretaceous Thermal Maximum; Deccan = Deccan volcanism event, PETM = Paleocene/Eocene Thermal Maximum, and MECO = Middle Eocene Climatic Optimum; and (5) Earth's greenhouse climatic state. Dashed vertical line at 1.8‰ is threshold value used by Miller et al. (1987) for middle bathyal benthic foraminiferal $\delta^{18}O$ values to mark Paleogene transition from ice-free to ice sheet conditions in Antarctica.

deep waters in the Pacific, Indian, or North Atlantic at least until the Maastrichtian (Fig. 9). SHL benthic $\delta^{13}C$ values are higher by 1–2‰ than in the other regions from the Turonian through the Campanian suggesting either SHL deep waters were largely isolated from deeper water in other oceans or that any flow between regions would be toward SHL. Circulation patterns inferred from neodymium isotopes (ϵ_{Nd}) support the idea that the SHL was not a source region for intermediate or deep waters for most of the Cretaceous. Whereas ϵ_{Nd} trends in North Atlantic, Pacific and Tethyan sites indicate changing Late Cretaceous circulation patterns among Atlantic, Pacific, Tethyan, and Boreal waters (Dameron et al., 2017; Frank et al., 2005; Jiménez Berrocoso et al., 2010; MacLeod et al., 2008; Martin et al., 2012; Pucéat et al., 2005; Zheng et al., 2013), analogous studies of SHL sites find highly variable ϵ_{Nd} values and trends that were attributed to local inputs and internal circulation in the region at least until the Campanian (Moiroud et al., 2016; Murphy and Thomas, 2012; Robinson et al., 2010; Robinson and Vance, 2012; Thomas et al., 2014; Voigt et al., 2013).

During the late Campanian to Maastrichtian, planktonic and benthic $\delta^{13}C$ values converge, benthic $\delta^{13}C$ increase to values similar to or above values in other basins, and planktonic $\delta^{18}O$ values increase. At the same time, SHL ϵ_{Nd} values converge. Together, these observations suggest deep circulation in SHL became better connected both internally and with other basins coincident with cooling temperatures and the

transition away from the Late Cretaceous greenhouse interval (e.g., MacLeod and Huber, 1996; Robinson et al., 2010; Voigt et al., 2013).

Finally, relative to other regions, SHL $\delta^{18}O$ trends (Fig. 9) seem to best approximate the traditional characterization of Late Cretaceous climate evolution with warming from the Albian through the Cenomanian followed by a hot greenhouse interval that spans the Turonian to Santonian before a gradual and progressive cooling during the Campanian and Maastrichtian (e.g., Douglas and Savin, 1975; Savin, 1977; Huber et al., 1995, 2002; Cramer et al., 2009; Friedrich et al., 2012; O'Brien et al., 2017). In other regions, patterns vary in the timing and pattern of cooling. Stable isotope results from Exmouth Plateau (Falzoni et al., 2016; Indian Ocean trend on Fig. 9) indicate that cooling began in the Coniacian and effectively stabilized by the middle of the Campanian. Long-term Pacific planktonic trends are not available, but Pacific benthic $\delta^{18}O$ values also show no long-term trends from the late Campanian onwards. Big gaps from the early through middle Campanian record at Blake Nose (Huber et al., 2002) complicate its use as representative of the North Atlantic as do potential diagenetic concerns (MacLeod et al., 2005), but these problems are mitigated by the fact that TEX$_{86}$ trends from the U.S. Gulf Coast (Linnert et al., 2014) and Demerara Rise (Forster et al., 2007) support and fill in gaps in the Blake Nose record. Together, data from these sites indicate that North Atlantic surface cooling effectively ended by the middle Campanian.
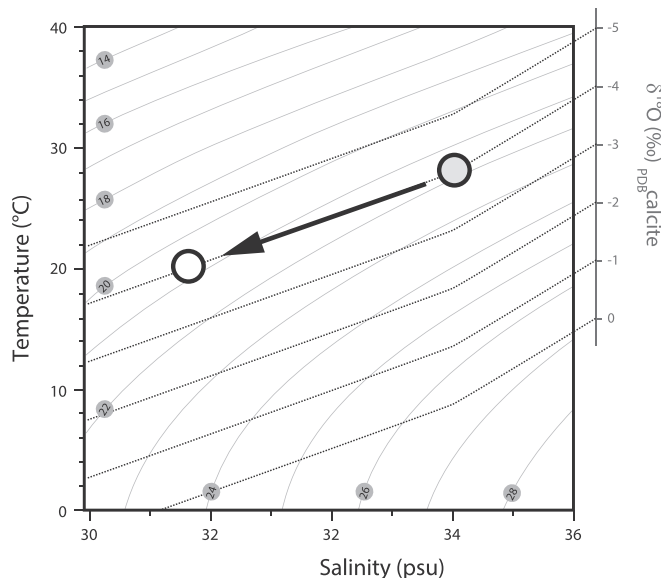
Fig. 8. Relationships between the oxygen isotopic composition of calcite as a function of the temperature, salinity, and density of seawater using the model of (Railsback et al., 1989). Numbers in the gray circles are values for density (in σ_t units) for the isopycnals, which are shown as gray lines. Isopleths of δ^{18}O planktonic foraminiferal calcite are calculated in equilibrium (dotted lines) using the paleotemperature equation of Kim and O'Neil, 1997; as reformulated by Bemis et al., 1998) assuming (1) that water with a salinity of 34 psu had a δ^{18}O composition of $-1‰_{SMOW}$ (appropriate for an ice-free world), (2) fresh water inputs had a value of $-20‰$ $_{SMOW,}$ and (3) the evaporative fraction was 0.63‰/psu (Huber et al., 2011).

4.3. Threshold for ice sheet growth

The existence of ice sheets in Antarctica during the Cretaceous has been debated for many years. On one hand, faunal and floral evidence for high latitude warmth has led many to consider the Late Cretaceous as too warm and equable to support ice sheets. Therefore, calculations of Cretaceous oxygen isotope paleotemperatures commonly assume ice-free conditions (Barron et al., 1981; Barron and Washington, 1985; Savin et al., 1975; Shackleton and Kennett, 1975). On the other hand, sequence stratigraphic studies have suggested that globally correlatable rapid sea level falls of at least 50 m during the Cretaceous must have been caused by the buildup of ice on Antarctica (Vail et al., 1977; Haq et al., 1987; Miller et al., 2005; Müller et al., 2016).

The only direct evidence for glacial ice during the Cretaceous is a possibly Valanginian (Early Cretaceous) tillite discovered in the Cadna-owie Formation in the northern Flinders Range of South Australia, (Alley and Frakes, 2003), which was located at 75 °S paleolatitude. Slightly younger striated boulders with chatter marks and polished surfaces found in association with the Bulldog Shale Member in the NE Flinders Range have been interpreted as having been deposited during glacial events in the mid- to late Aptian and early to middle Albian (Alley et al., 2011). However, the glacial origin of the boulders remains unproven since they occur adjacent to, rather than within, the Bulldog Shale outcrop and the Valanginian age is based on palynomorphs obtained from units that overlie rather than occur within the tillite bed.

Coordinated positive shifts in Cretaceous planktonic and benthic foraminiferal δ^{18}O records that occur at levels of sea level fall would provide secondary evidence for ice sheet growth (Prentice and Matthews, 1991) and such evidence has been proposed for events in the mid-Cenomanian (~95 Ma) and the early Turonian (~91 Ma; Miller et al., 2004, 2005; Bornemann et al., 2008). More detailed study, though, has shown the proposed correlation fails tests at higher spatial and temporal resolution (Ando et al., 2009; MacLeod et al., 2013; Moriya et al., 2007) and is not supported by climate modeling studies

(Ladant and Donnadieu, 2016). Further, the accuracy of cited eustatic curves during the late Cenomanian through Turonian has been questioned with alternative dating and regional forcing proposed for key events (Haq and Huber, 2017).

The best candidate for a time with Late Cretaceous ice sheets is the early Maastrichtian. Like above, proposals that a small ice sheet formed during the early Maastrichtian are founded on purported synchroneity between sea level events and positive increases in foraminiferal δ^{18}O values (Barrera, 1994; Barrera and Savin, 1999; Barrera et al., 1997; Miller et al., 1999). However, uncertainty in age correlations of the sea-level events, inconsistency in the timing of δ^{18}O data trends among different locations, and lack of sedimentological evidence of contemporary glaciation cast doubt on the conclusions (MacLeod and Huber, 2001). Unlike the mid-Cenomanian and early Turonian, though, bathyal temperatures inferred from early Maastrichtian benthic δ^{18}O are at a Late Cretaceous minimum (Figs. 6, 7), climate model simulations exist that favor perennial ice accumulation (Ladant and Donnadieu, 2016), and seasonal sea ice has been proposed to have existed based on sedimentological and paleontological evidence from the Arctic (Davies et al., 2009; Ladant and Donnadieu, 2016) and Antarctic (Bowman et al., 2013). Still, no glacial deposits have been found.

Foraminiferal δ^{18}O records alone can place few firm constraints on when or if ice sheets were present during greenhouse climates, but knowing what benthic values correspond to times of ice sheet growth and which correspond to ice-free conditions would help establish thresholds for when transitions might occur. Ice sheets formed and grew as the late Eocene climate cooled, and a large East Antarctic ice sheet eventually advanced to sea level while benthic foraminiferal δ^{18}O values increased. A critical value for middle bathyal benthic foraminifera has been proposed as 1.8‰ (Miller et al., 1987, 2005). Benthic foraminiferal δ^{18}O measurements from Kerguelen Plateau (southern Indian Ocean) reach this value by ~35 Ma, which coincides with a sharp increase in ice-rafted debris (IRD) (Barron et al., 1991; Wise Jr. et al., 1992; Zachos et al., 1992). Latest Eocene benthic foraminiferal δ^{18}O values from Maud Rise range between 1.0‰ and 1.6‰ and increase to 2.6‰ by the time the East Antarctic ice sheet formed in the early Oligocene (Stott and Kennett, 1990; Mackensen and Ehrmann, 1992; Fig. 7). The oldest Cenozoic IRD was reported from late middle Eocene (~45–44 Ma) sediments on Kerguelen Plateau and Maud Rise (Ehrmann and Mackensen, 1992). Corresponding δ^{18}O values at Maud Rise for that time range between 1.0 and $-0.5‰$, which is comparable to the range of values at Maud Rise during the Maastrichtian. Note, though, that differences in palaeogeography, moisture sources, transport pathways, altitude of ice formation, and CO_2 thresholds all affect ice sheets (Linnert et al., 2014; Ladant and Donnadieu, 2016). Thus, while Maastrichtian benthic foraminiferal δ^{18}O values approach those from Paleogene times of known ice build-up, caution should be used in deciding whether or not this similarity signifies ice existed in the Late Cretaceous.

Cool temperatures inferred from fossils collected in shallow marine deposits on Seymour Island (northeast Antarctic Peninsula), located at ~62 °S paleolatitude (Müller et al., 2016), continue to fuel speculation on the presence of Cretaceous greenhouse glaciers. The δ^{18}O values of Maastrichtian mollusks yield a wide range of values within the last 4 m.y. of the Maastrichtian, with coolest mean temperatures ranging from 4 to 6 °C (Tobin et al., 2012). These values compare well with coolest temperature estimates from several benthic foraminiferal species (Barrera et al., 1987), but they differ in that the foraminiferal records show no discernable stratigraphic trend while the mollusk data suggest a slight warming toward the end of the Maastrichtian. Clumped isotope analyses of a subset of the Tobin et al. (2012) samples, on the other hand, suggested more dramatic temperature swings than inferred because of correlated changes in temperatures and local seawater δ^{18}O values that tended to cancel each other out (Petersen et al., 2016). Kemp et al. (2014) also suggest cool temperatures (8 to 12 °C ± 5 °C)
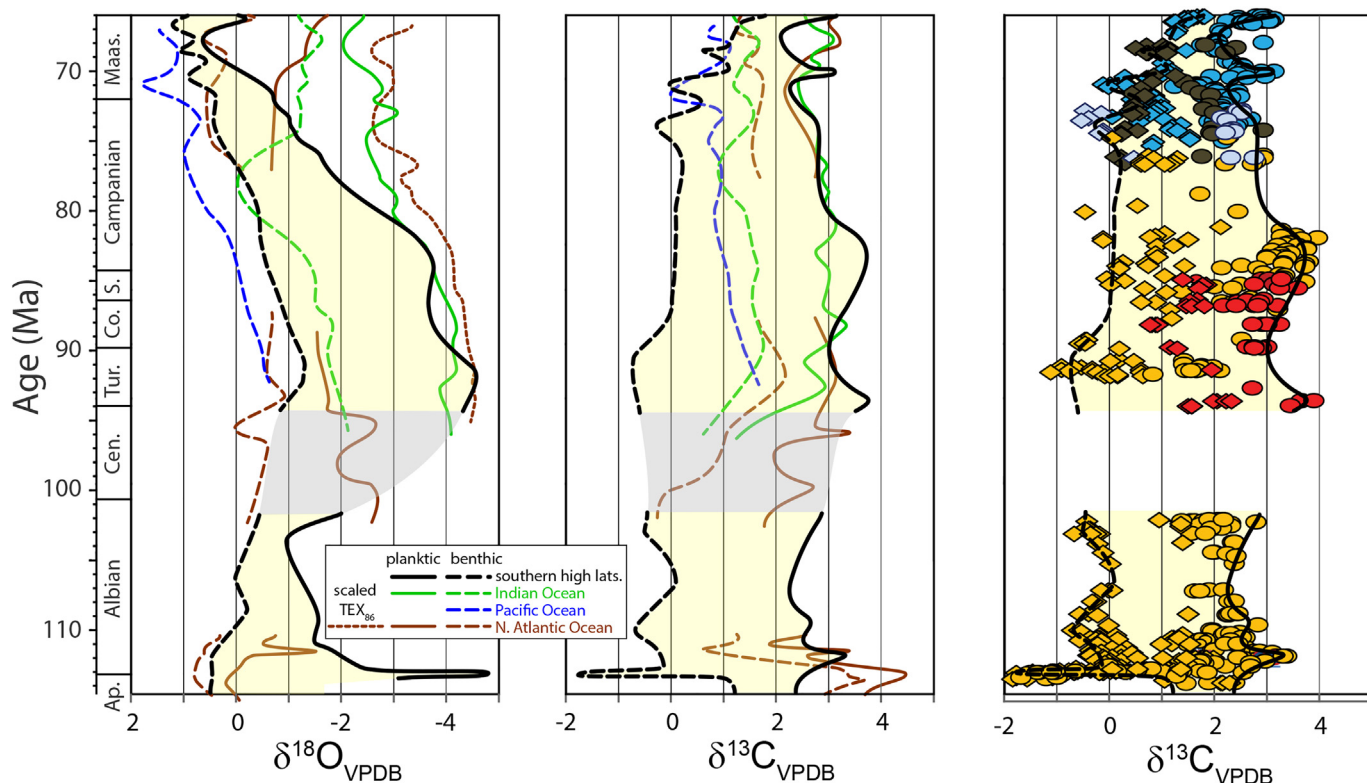
**Fig. 9.** Late Cretaceous planktonic and benthic foraminiferal δ ^{18}O values (left panel) and δ ^{13}C values (center panel) plotted against age illustrating regional differences in isotopic trends and large changes in the planktonic to benthic isotopic gradient at southern high latitudes (SHL) through time. Compiled data for each region were plotted on a common age axis constructed by interpolating between reported Age boundaries. A qualitative fit was then drawn to present a simplified depiction of trends through time. The right hand panel shows a representative plot of this approach applied to the SHL δ ^{13}C data from Fig. 6. Different regions are shown by different colors. Black lines depict SHL trends with yellow shading between curves included to emphasize changes in gradients between the sea surface and the sea floor gradients at SHL; gray band indicates Cenomanian interval where data are effectively absent for SHL. Other regions and data sources are brown- North Atlantic (Huber et al., 2002; MacLeod et al., 2005; Linnert et al., 2014), blue- subtropical Pacific (Friedrich et al., 2012; Ando et al., 2013), and green- Exmouth Plateau in the subtropical Indian Ocean (Falzoni et al., 2016). Solid lines represent trends in planktonic δ^{18}O values; dashed lines, benthic values; dotted brown line in δ ^{18}O plot trend in expected North Atlantic δ ^{18}O values estimated from TEX$_{86}$-based temperature estimates for surface water (see text). (For interpretation of the references to colour in this figure legend, the reader is referred to the web version of this article.)

for the latest Cretaceous on Seymour Island using the MBT/CBT (methylation index of branched tetraethers/cyclization ratio of branched tetraethers) paleothermometer. Analyses of growth rings from Seymour Island fossil wood were tentatively interpreted to indicate late Maastrichtian temperatures between 4 and 8 °C (Francis and Poole, 2002). However, several uncertainties, including taxonomic biases, tree competition, tree maturity, and moisture availability, limit reliability of temperature estimates using this proxy (Creber and Chaloner, 1984). Finally, peaks in abundance of a dinoflagellate resting cyst, also from the Maastrichtian sequence on Seymour Island, were interpreted to represent times of sea ice formation based on weak correlation with the Tobin et al. (2012) molluscan δ^{18}O dataset and speculative paleobiologic assumptions (Bowman et al., 2013, 2014). Considering sedimentologic evidence for glaciation or sea level change has never been found in the intensively studied and extensively exposed Seymour Island sequence (e.g., Askin, 1988; Huber, 1988; Macellari, 1988), proposals for ice sheet growth in the Antarctic Peninsula region remain unsupported.

In the absence of direct evidence for ice sheets at any time during the mid-Late Cretaceous, the next strongest possible support for the presence of ice sheets would be well documented synchroneity between positive shifts in δ^{18}O from biogenic carbonate and/or phosphate and sea level falls across a wide geographic range and different paleoenvironments which has not yet been demonstrated. Absence of such evidence indicates that if Cretaceous ice sheets existed, their size was too small to have affected at a resolvable level and on a global scale both the oxygen isotopic composition of the ocean and changes sea

level given current limitations of correlation.

5. Implications for cretaceous climate forcing mechanisms

The importance of atmospheric carbon dioxide concentrations (pCO$_2$) in regulating global temperature variations throughout the Phanerozoic has been accepted for more than a century (Arrhenius, 1896; Arthur et al., 1985; Budyko and Ronov, 1979; Chamberlin, 1899; Barron and Washington, 1985; Hay, 2008, 2011). Natural shifts in pCO$_2$ have primarily been influenced by changes in the relative rates of volcanic outgassing, chemical weathering of silicate rocks, and organic carbon burial. Periods of intensified oceanic crust formation, LIP activity, and/or arc production rates lead to a buildup of pCO$_2$ and increased global temperatures (Coffin and Eldholm, 1994; Larson, 1991b; Coffin et al., 2006), while times of intensified continent-continent plate collision result in increased chemical weathering rates, a drawdown of pCO$_2$, and cooler global temperatures (e.g., Raymo, 1991; Raymo et al., 1988). Obtaining accurate records of ancient temperature and pCO$_2$ changes and linking them to tectonic forcing mechanisms have been a major challenge for climate scientists because of ambiguities or uncertainties in the reliability of proxies used to reconstruct past temperatures and pCO$_2$ concentrations and incomplete information on the timing and rates of global tectonic events.

Comparison of the oxygen isotope paleotemperature compilation for the Cretaceous southern high latitudes with estimates of variation in pCO$_2$, crustal production at mid-ocean ridges and (LIPs), and lengths of continental and island arcs (Fig. 6) demonstrates that links between

Cretaceous temperature variations and any individual primary forcing factors are not well established. In particular, the proxies used to estimate Cretaceous pCO$_2$ show significant inconsistencies among methods and variable degrees of correlation to long-term paleotemperature trends. For example, the hot greenhouse temperatures of the Turonian correlate with a period of relatively low pCO$_2$ according to the fossil conifer leaf and stomatal index proxies, while the cooler temperatures of the Albian correlate with a time of higher pCO$_2$ according to the stomatal and liverwort indices but lower pCO$_2$ according to the fossil conifer pCO$_2$ proxy. Large uncertainties regarding the influence of moisture and sunlight availability, on leaf stomata density and metabolics, the δ^{13}C composition of the preserved organic matter and estimates of mean land surface temperatures used in pCO$_2$ estimates from soil carbonates may explain some of these discrepancies (Royer et al., 2014; Breecker et al., 2010; Foster et al., 2017).

Long-term variations in ^{87}Sr/^{86}Sr ratios of marine sediments track the relative importance and absolute rate of continental erosion vs. oceanic magmatism to the ocean's Sr budget with shifts moderated by erosion of older sedimentary rocks (Bralower et al., 1997; Jones et al., 1994; Larson, 1991a,b; McArthur et al., 2012). Higher ^{87}Sr/^{86}Sr ratios are taken to indicate dominance of continental mountain building and chemical weathering while lower ratios indicate increased oceanic magmatism and/or erosion of large basaltic provinces on land. The mean seawater ^{87}Sr/^{86}Sr curve (Fig. 6) shows generally good agreement with the paleotemperature compilation, with lowest values occurring during the hot greenhouse temperatures in the Turonian-Santonian and ratios that increase minimum values during the Maastrichtian when temperatures were coolest.

Changes in rates of Cretaceous oceanic crust production (Müller et al., 2016), in the timing of formation of LIP (Coffin et al., 2006), and in lengths of subduction-related volcanic arcs (van der Meer et al., 2014), correspond to variations in Cretaceous SHL temperatures in some time intervals, but not in others (Fig. 6). The largest short-term variation in oceanic crustal production rate in the ~115 to ~66 Ma interval, a decrease of ~8 km^3/yr between ~100 and ~98 Ma (Matthews et al., 2012), occurred during a gap in the SHL δ^{18}O record. However, the decrease in δ^{18}O values between ~102 and ~94 Ma argues for increased temperatures, the opposite of the expected impact of a decrease in oceanic crustal production and associated lower CO$_2$ degassing rates. Similarly, the overall trend of increasing oceanic crustal production rates from ~98 to ~65 Ma corresponds to the long-term trend of decreasing temperatures from the Turonian to the Maastrichtian. In contrast, a peak in LIP production and associated CO$_2$ degassing between ~100 and ~95 Ma corresponds well with the decrease in δ^{18}O values between ~102 and ~94 Ma arguing for increased temperatures. Otherwise, the overall trend of decreasing LIP production rates from ~95 to ~66 Ma agrees with the overall trend of decreasing temperatures in the same time interval. Subduction-related volcanic arc lengths, a proxy for arc crustal production and associated CO$_2$ degassing, show an overall decrease from ~115 to ~65 Ma, whereas temperatures increase between ~102 and ~94 Ma but decrease from ~95 to ~66 Ma.

Correspondence between the timing of peak volcanism at the Deccan Traps (southwest India) and global warming provides strong support for volcanic CO$_2$ as the trigger for a warming event during the late Maastrichtian. Magma eruption rates for the Deccan Event were highest during the late Maastrichtian, ~150–300 k.y. before the Cretaceous/Paleogene boundary (Ravizza et al., 2001; Robinson et al., 2009; Renne et al., 2015; Font et al., 2016), which coincides with a 2.5–5 °C temperature increase estimated from δ^{18}O measurements from deep sea benthic foraminifera from multiple equatorial, mid-latitude and high latitude locations (Barrera, 1994; Barrera and Savin, 1999; Huber et al., 2002; Westerhold et al., 2011; Barnet et al., 2018) and an estimated warming of ~3 °C on Seymour Island, Antarctica (Tobin et al., 2012). This event is well-delineated between 66.5 and 66.2 Ma with an ~4 °C warming of SHL at ODP Site 690 (Barrera and Savin, 1999), as shown in Figs. 6 and 7.

Inconsistencies between the timing of elevated rates of tectonic sources of CO$_2$ and evidence for increased SHL warming (Fig. 6) can be attributed to multiple factors, including uncertainties in: (1) the rates of lithosphere production and consumption (van der Meer et al., 2014), (2) the amount of carbon concentrated in descending slabs and decarbonation efficiency at subduction zones (Johnston et al., 2011), (3) estimates of the timing and volume of magma production during LIP eruptions (Coffin et al., 2006), (4) estimates for the amount of CO$_2$ released from various types of volcanoes (Burton et al., 2013), (5) estimates of the length of island arcs (van der Meer et al., 2014), and (6) estimates of weathering rates of volcanic and non-volcanic rocks (Berner, 2006). These inconsistencies and uncertainties will diminish as gaps in the SHL oxygen isotope paleotemperature curve are filled and constraints on changing pCO$_2$ that integrate pooled estimates for mantle derived and oxidized organic carbon CO$_2$ sources as well as weathering and organic carbon burial sinks improve.

6. Conclusions

New benthic and planktonic foraminiferal δ^{18}O data from the southern Indian Ocean (Mentelle Basin DSDP Site 258) confirm low to extremely low δ^{18}O values previously reported for the southern South Atlantic (Falkland Plateau DSDP Sites 511 and 327) and strengthen the argument that the Cretaceous Hot Greenhouse was considerably warmer than its Cenozoic counterpart. At Site 258 warmest temperatures occur within the lowermost Turonian and just above a black shale bed that is correlated with Oceanic Anoxic Event 2. These new data undermine arguments that Falkland Plateau results are anomalous due to local oceanographic and/or sedimentological conditions. If regional seawater had δ^{18}O values close to the canonical ice-free value of -1‰$_{SMOW}$, Turonian foraminiferal δ^{18}O values imply surface water temperatures > 27 °C and bottom water temperatures > 19 °C. Such extreme warmth at 58–60°S seems improbable and an alternative possibility is that SHL δ^{18}O values were at least partially influenced by higher precipitation rates and a steeper trend in the seawater latitudinal δ^{18}O gradient.

The δ^{18}O trends at SHL seem to best approximate the traditional characterization of Late Cretaceous climate evolution with warming from the Albian through the Cenomanian, followed by peak warmth during the KTM and sustained warmth through the Santonian before a gradual and progressive cooling during the Campanian and Maastrichtian. We find no compelling evidence for ice sheets of significant size at any time during this entire time. Compilations of δ^{18}O paleotemperature data from the SHL (this study) and other global δ^{18}O and TEX$_{86}$ compilations (e.g., Huber et al., 2002; Pucéat et al., 2005; Cramer et al., 2009; Friedrich et al., 2012; O'Brien et al., 2017) along with climate modeling studies (Ladant and Donnadieu, 2016) all indicate that the Cretaceous Hot Greenhouse (Turonian-Santonian) was too warm to support polar ice sheets except possibly at the highest altitudes in Antarctica. Even during the coolest times of the mid-Late Cretaceous (late Aptian and mid-Maastrichtian), absence of glacial deposits, of coordinated positive shifts in Cretaceous planktonic and benthic foraminiferal δ^{18}O records and of corresponding eustatic falls in sea level cast doubt on recurring proposals for the existence of polar ice sheets during those times (e.g., Barrera, 1994; Barrera and Savin, 1999; Barrera et al., 1997; Miller et al., 1999; Bowman et al., 2013, 2014).

Throughout the Cretaceous Hot Greenhouse the SHL sites show high surface-to-depth gradients in δ^{18}O and δ^{13}C and lower benthic δ^{13}C values than have been documented at lower latitudes. Regionally divergent trends in Cretaceous δ^{18}O and δ^{13}C datasets probably reflect different degrees of connectivity among the Cretaceous ocean basins. Further studies that characterize deep ocean circulation patterns inferred from neodymium isotopes integrated with geochemical paleotemperature proxies and sedimentological data, as well as recovery of missing sections spanning most of the Cenomanian and mid-

Campanian, are needed to establish a fuller understanding of the evolution of the Cretaceous climate-ocean system at SHL and their relationship to changes in global deep-water circulation patterns.

The role of pCO$_2$ and other greenhouse gases in regulating global climate is a long-established paradigm (see review above). However, predicted correlations between forcing mechanisms (mainly high CO$_2$ degassing rates during high rates of ocean crust and LIP production and global subduction) do not consistently line up with SHL temperature trends. Counterbalancing effects of increased chemical weathering of silicate rocks and increased organic carbon burial may account for some or all of the mismatch between temperature and CO$_2$ production estimates. Unfortunately, pCO$_2$ proxies currently do not have high enough fidelity to resolve the CO$_2$ changes through time sufficiently to advance study of sources and sinks. Obtaining more accurate records of ancient temperature and pCO$_2$ changes and linking them to tectonic forcing mechanisms is necessary for climate modelers and the geologic community to remove ambiguities or uncertainties in the reliability of proxies used to reconstruct past temperatures and pCO$_2$ concentrations and the timing and rates of global tectonic events.

Acknowledgements

References

Alley, N.F., Frakes, L.A., 2003. First known cretaceous glaciation: Livingston Tillite member of the Cadna-owie formation, South Australia. Aust. J. Earth Sci. 50, 139–144.

Alley, N.F., Frakes, L.A., Sheard, M.J., Gray, D., 2011. Unravelling Early Cretaceous Glacial Events in the Southern Eromanga Basin: Evidence from the Cadna-Owie Formation and Bulldog Shale, 6th Sprigg Symposium. vol. 100. Geological Society of Australia, Adelaide, pp. 1–4.

Ando, A., Kakegawa, T., Takashima, R., Saito, T., 2002. New perspective on Aptian carbon isotope stratigraphy: data from δ^{13}C records of terrestrial organic matter. Geology 30, 227–230.

Ando, A., Huber, B.T., MacLeod, K.G., Ohta, T., Khim, B.-K., 2009. Blake Nose stable isotopic evidence against the mid-Cenomanian glaciation hypothesis. Geology 37, 451–545. http://dx.doi.org/10.1130/G25580A.

Ando, A., Woodard, S.C., Evans, H.F., Littler, K., Herrmann, S., MacLeod, K.G., Kim, S., Khim, B.-K., Roginson, S.A., Huber, B.T., 2013. An emerging palaeoceanographic 'missing link': multidisciplinary study of rarely recovered parts of deep-sea Santonian–Campanian transition from Shatsky Rise. J. Geol. Soc. 170, 381–384.

Arrhenius, S., 1896. On the Influence of Carbonic Acid in the Air upon the Temperature of the Ground: Philosophical Magazine. 41. pp. 237–276.

Arthur, M.A., Dean, W.E., Schlanger, S.O., 1985. Variations in the Global Carbon Cycle during the Cretaceous Related to Climate, Volcanism, and Changes in Atmospheric CO$_2$. In: Proceedings the Carbon Cycle and Atmospheric CO$_2$: Natural Variations Archaen to Present: Washington, D.C., American Geophysical Union, Geophysical Monograph. Vol. 32. pp. 504–529.

Arthur, M.A., Dean, W.E., Pratt, L.M., 1988. Geochemical and climatic effects of increased marine organic carbon burial at the Cenomanian/Turonian boundary. Nature 335, 714–717.

Askin, R.A., 1988. Campanian to Eocene palynological succession of Seymour and adjacent islands, northeastern Antarctic Peninsula. In: Feldmann, R.M., Woodburne, M.O. (Eds.), Geology and Paleontology of Seymour Island, Antarctic Peninsula. Vol. 169. Geological Society of America, pp. 131–153 Memoir Series.

Barker, P.F., Kennett, J.P., Shipboard Scientific Party, 1988. Proceedings of the Ocean Drilling Program, Initial Reports, Volume 113. 15. Phanerozoic: Geochemistry International, College Station, TX, Ocean Drilling Program, pp. 1–9 p. 785.

Barnet, J.S.K., Littler, K., Kroon, D., Leng, M.J., Westerhold, T., Röhl, U., Zachos, J.C., 2018. A new high-resolution chronology for the late Maastrichtian warming event: Establishing robust temporal links with the onset of Deccan volcanism. Geology 46 (2), 147–150.

Barral, A., Gomez, B., Fourel, F., Daviero-Gomez, V., Lécuyer, C., 2017. CO$_2$ and temperature decoupling at the million-year scale during the cretaceous greenhouse. Nat. Commun. 7 (8310).

Barrera, E., 1994. Global environmental changes preceding the cretaceous-tertiary boundary: early-late Maastrichtian transition. Geology 22, 877–880.

Barrera, E., Huber, B.T., 1990. Evolution of Antarctic waters during the Maestrichtian: foraminifer oxygen and carbon isotope ratios, ODP Leg 113. In: Barker, P.F., Kennett, J.P. (Eds.), Proceedings of the Ocean Drilling Program, Scientific Results. 113. Ocean Drilling Program, College Station, TX, pp. 813–823.

Barrera, E., Savin, S.M., 1999. Evolution of late Campanian-Maastrichtian marine climates and oceans. In: Barrera, E., Johnson, C. (Eds.), Evolution of the Cretaceous Ocean-Climate System: Boulder, CO, Geological Society of America Special Paper. Vol. 332. pp. 245–282.

Barrera, E., Huber, B.T., Savin, S.M., Webb, P.N., 1987. Antarctic marine temperatures: late Campanian through early Paleocene. Paleoceanography 2, 21–47.

Barrera, E., Savin, S.M., Thomas, E., Jones, C.E., 1997. Evidence for thermohaline-circulation reversals controlled by sea-level change in the latest cretaceous. Geology 25, 715–718.

Barron, E.J., Washington, W.M., 1985. Warm Cretaceous climates: high atmospheric CO$_2$ as a plausible mechanism. In: Sundquist, E.T., Broecker, W.S. (Eds.), The Carbon Cycle and Atmospheric CO$_2$: Natural Variations Archaen to Present, American Geophysical Union, Geophysical Monograph no. Vol. 32. pp. 546–553.

Barron, E.J., Thompson, S.L., Schneider, S.H., 1981. An ice-free cretaceous? Results from climate model simulations. Science 212, 501–508.

Barron, J.A., Larsen, B., Baldauf, J.G., 1991. Evidence for late Eocene to early Oligocene Antarctic glaciation and observations on late Neogene glacial history of Antarctic: results from leg 119. In: Barron, J.A., Larsen, B.L., Baldauf, J.G. (Eds.), Proceedings of the Ocean Drilling Program, Scientific Results. 119. College Station, TX, Ocean Drilling Program, pp. 869–891.

Basov, I.A., Krasheninnikov, V.A., 1983. Benthic foraminifers in Mesozoic and Cenozoic sediments of the southwestern Atlantic as an indicator of paleoenvironment, deep-sea drilling project leg 71. In: Ludwig, W.J., Krasheninnikov, V.A. (Eds.), Initial Rep. Deep Sea Drill. Proj. 71. U.S. Government Printing Office, Washington, D.C., pp. 739–787.

Bemis, B.E., Spero, H.J., Bijma, J., Lea, D.W., 1998. Reevaluation of the oxygen isotopic composition of planktonic foraminifera: experimental results and revised paleotemperature equations. Paleoceanography 13, 150–160.

Berner, R.A., 2006. Inclusion of the weathering of volcanic rocks in the GEOCARBSULF model. Am. J. Sci. 306 (5), 295–302.

Bice, K.L., Huber, B.T., Norris, R.D., 2003. Extreme Polar Warmth during the Cretaceous Greenhouse? The Paradox of the Late Turonian δ^{18}O Record at DSDP Site 511: Paleoceanography, V. Vol. 18. pp. 1031. http://dx.doi.org/10.1029/2002PA000848.

Bohaty, S.M., Zachos, J.C., 2003. Significant Southern Ocean warming event in the late middle Eocene. Geology 31, 1017–1020.

Bohaty, S.M., Zachos, J.C., Florindo, F., Delaney, M.L., 2009. Coupled greenhouse warming and deep-sea acidification in the middle Eocene: paleoceanography. 24 (PA2207), 1–16.

Bornemann, A., Norris, R.D., Friedrich, O., Beckmann, B., Schouten, S., Sinninghe Damsté, J.S., Vogel, J., Hofmann, P., Wagner, T., 2008. Isotopic evidence for glaciation during the Cretaceous Supergreenhouse. Science 319, 189–192.

Bowman, V.C., Francis, J.E., Riding, J.B., 2013. Late cretaceous winter sea ice in Antarctica? Geology 41 (12), 1227–1230.

Bowman, V.C., Francis, J.E., Askin, R.A., Riding, J.B., Swindles, G.T., 2014. Latest cretaceous–earliest Paleogene vegetation and climate change at the high southern latitudes: palynological evidence from Seymour Island, Antarctic peninsula. Palaeogeogr. Palaeoclimatol. Palaeoecol. 408, 26–47.

Bralower, T.J., Fullagar, P.D., Paull, C.K., Dwyer, G.S., Leckie, R.M., 1997. Mid-Cretaceous Strontium-Isotope Stratigraphy of Deep-Sea Sections. Vol. 109. Geological Society of America Bulletin, pp. 1421–1442.

Breecker, D.O., Sharp, Z.D., McFadden, L.D., 2010. Atmospheric CO$_2$ concentrations during ancient greenhouse climates were similar to those predicted for A.D. 2100. Proc. Natl. Acad. Sci. 107, 576–580.

Brouwers, E.M., Clemens, W.A., Spicer, R.A., Ager, T.A., Carter, L.D., Sliter, W.V., 1987. Dinosaurs on the north slope, Alaska: high latitude, latest cretaceous environments. Science 237, 1608–1610.

Budyko, M.I., Ronov, A.B., 1979. Chemical Evolution of the Atmosphere in the.

Burton, M.R., Sawyer, G.M., Granieri, D., 2013. Deep carbon emissions from volcanoes. Rev. Mineral. Geochem. 75, 323–354.

Carter, A., Riley, T.R., Hillenbrand, C.-D., Riggner, M., 2017. Widespread Antarctic glaciation during the Late Eocene. Earth Planet. Sci. Lett. 458, 49–57.

Case, J.A., 1988. Paleogene floras from Seymour Island, Antarctic Peninsula. In: Feldmann, R.M., Woodburne, M.O. (Eds.), Geology and Paleontology of Seymour Island, Antarctic Peninsula. 169. Geological Society of America, Memoir Series, pp. 523–530.

Case, J.A., Martin, J.E., Chaney, D.S., Reguero, M., Marenssi, S.A., Santillana, S.M., Woodburne, M, O., 2000. The first duck-billed dinosaur (Family Hadrosauridae) from Antarctica. J. Vertebr. Paleontol. 20, 612–614.

Chamberlin, T.C., 1899. An attempt to frame a working hypothesis of the cause of glacial periods on an atmospheric basis. J. Geol. 7 (667–685), 751–787 p. 545–584.

Clarke, L.J., Jenkyns, H.C., 1999. New oxygen isotope evidence for long-term Cretaceous climatic change in the Southern Hemisphere. Geology 27, 699–702.

Coffin, M.F., Eldholm, O., 1994. Large igneous provinces: crustal structure, dimensions, and external consequences. Rev. Geophys. 32, 1–36.

Coffin, M.F., Duncan, R.A., Eldholm, O., Fitton, J.G., Frey, F.A., Larsen, H.C., Mahoney, J.J., Saunders, A.D., Schlich, R., Wallace, P.J., 2006. Large igneous provinces and scientific ocean drilling. Oceanography 19, 150–160.

Cramer, B.S., Toggweiler, T.R., Wright, J.D., Katz, M.E., Miller, K.G., 2009. Ocean overturning since the Late Cretaceous: Inferences from a new benthic foraminiferal isotope compilation. Paleoceanography 24, Pa4216. http://dx.doi.org/10.1029/2008PA001683.

Creber, G.T., Chaloner, W.G., 1984. Influence of environmental factors on the wood structure of living and fossil trees. Bot. Rev. 50, 357–448.

Crowley, T.J., 1991. Past CO2 changes and tropical sea surface temperatures. Paleoceanography 6, 387–394.

Crowley, T.J., Berner, R.A., 2001. CO2 and climate change. Science 292, 870–872.

Dameron, S.N., Leckie, R.M., Clark, K., MacLeod, K.G., Thomas, D.J., Lees, J.A., 2017. Extinction, dissolution, and possible ocean acidification prior to the Cretaceous/Paleogene (K/Pg) boundary in the tropical Pacific. Palaeogeogr. Palaeoclimatol. Palaeoecol. 485, 433–454.

Davies, T.A., Luyendyk, B.P., Shipboard Scientific Party, 1974. Initial Reports of the Deepsea Drilling Project. vol. 26 U.S. Government Printing Office, Washington, D.C. (1129 pp.).

Davies, A., Kemp, A.E.S., Pike, J., 2009. Late Cretaceous seasonal ocean variability from the Arctic. Nature 460, 254–259.

van der Meer, D., Zeebe, R.E., van Hinsbergen, D.J.J., Sluis, A., Spakman, W., Torsvik, T.H., 2014. Plate tectonic controls on atmospheric CO2 levels since the Triassic. Proceed. Nat. Acad. Sci. 111 (12), 4380–4385.

Donnadieu, Y., Pucéat, E., Moir, Moirod, M., Guillocheau, F., Deconinck, J.F., 2016. A betterventilated ocean triggered by Late Cretaceous changes in continental configuration. Nat. Commun. 7 (10316), 1–12.

Douglas, R.G., Savin, S.M., 1975. Oxygen and carbon isotope analyses of Tertiary and Cretaceous microfossils from the Shatsky Rise and other sites in the North Pacific Ocean. In: Larson, R.L., Moberly, R. (Eds.), Initial Reports of the Deep-sea Drilling Project. vol. 32. U.S. Govt. Printing Office, Washington, D.C., pp. 509–520.

Ehrmann, W.U., Mackensen, A., 1992. Sedimentological evidence for the formation of an East Antarctic ice sheet in Eocene/Oligocene time. Palaeogeogr. Palaeoclimatol. Palaeoecol. 93, 85–112.

Falzoni, F., Petrizzo, M.R., Jenkyns, H.C., Gale, A.S., Tsikos, H., 2016. Planktonic foraminiferal biostratigraphy and assemblage composition across the Cenomanian-Turonian boundary interval at Clot Chevalier (Vocontian Basin, SE France). Cretac. Res. 59, 69–97.

Fassell, M.L., Bralower, T.J., 1999. Warm, equable mid-Cretaceous: Stable isotope evidence. In: Barrera, E., Johnson, C. (Eds.), Evolution of the Cretaceous Ocean-Climate System. 332. Geological Society of America Special Paper, Boulder, CO, pp. 121–142.

Font, E., Adatte, T., Nbrega Sial, A., Drude de Lacerda, L., Keller, G., Punekar, J., 2016. Mercury anomaly, Deccan volcanism, and the end-Cretaceous mass extinction. Geology 44, 171–174.

Forster, A., Schouten, S., Moriya, K., Wilson, P.A., Sinninghe Damsté, J.S., 2007. Tropical warming and intermittent cooling during the Cenomanian/Turonian oceanic anoxic event 2: sea surface temperature records from the equatorial Atlantic. Paleoceanography 22, PA1219. http://dx.doi.org/10.1029/2006PA001349.

Foster, G.L., Royer, D.L., Lunt, D.J., 2017. Future climate forcing potentially without precedent in the last 420 million years. Nat. Commun. 8, 1–8.

Francis, J.E., Poole, I., 2002. Cretaceous and early Tertiary climates of Antarctica: evidence from fossil wood. Palaeogeogr. Palaeoclimatol. Palaeoecol. 182, 47–64.

Frank, T.D., Thomas, D.J., Leckie, R.M., Arthur, M.A., Bown, P.R., Jones, K., Lees, J., 2005. The Maastrichtian record from Shatsky Rise (northwest Pacific): a tropical perspective on global ecological and oceanographic changes. Paleoceanography 20, PA1008. http://dx.doi.org/10.1029/2004PA001052.

Friedrich, O., Schmiedl, G., Erlenkeuser, H., 2006. Stable isotope composition of Late Cretaceous benthic foraminifera from the southern South Atlantic: biological and environmental effects. Mar. Micropaleontol. 58, 135–157.

Friedrich, O., Norris, R.D., Erbacher, J., 2012. Evolution of middle to Late Cretaceous oceans–A 55 m.y. record of Earth's temperature and carbon cycle. Geology 40, 107–110. http://dx.doi.org/10.1130/G32701.32701.

Gale, A.S., Hardenbol, J., Hathway, B., Kennedy, W.J., Young, J.R., Phansalkar, V., 2002. Global correlation of Cenomanian (Upper Cretaceous) sequences: evidence for Milankovitch control on sea level. Geology 30, 291–294.

Gradstein, F.M., Ogg, J.G., Schmitz, M.D., Ogg, G.M., 2012. In: The Geologic Time Scale 2012. The Netherlands, Elsevier, Amsterdam, pp. 1144.

Gröcke, D.R., Hesselbo, S.P., Jenkyns, H.C., 1999. Carbon-isotope composition of Lower Cretaceous fossil wood: ocean-atmosphere chemistry and relation to sea-level change. Geology 27, 155–158.

Hamilton, N., 1990. Mesozoic magnetostratigraphy of Maud Rise, Antarctica. In: Barker, P.F., Kennett, J.P., Shipboard Scientific Party (Eds.), Proceedings of the Ocean Drilling Program, Scientific Results. vol. 113. Ocean Drilling Program, College Station, TX, pp. 255–260.

Haq, B.U., Huber, B.T., 2017. Anatomy of a eustatic event during the Turonian (Late Cretaceous) hot greenhouse climate. Sci. China Earth Sci. 60 (1), 20–29.

Haq, B.U., Hardenbol, J., Vail, P.R., 1987. The new chronostratigraphic basis of Cenozoic and Mesozoic sea level cycles. In: Ross, C.A., Haman, D. (Eds.), Timing and Depositional History of Eustatic Sequences: Constraints on Seismic Stratigraphy. Cushman Foundation Special Publication No. 24 pp. 7–13.

Hay, W.W., 2008. Evolving ideas about the Cretaceous climate and ocean circulation. Cretac. Res. 29, 725–753.

Hay, W.W., 2011. Can humans force a return to a "Cretaceous" climate? Sediment. Geol. 235, 5–26.

Herb, R., 1974. Cretaceous planktonic foraminifera from the eastern Indian Ocean. In: Davies, T.A., Luyendyk, B.P., Shipboard Scientific Party (Eds.), Initial Reports of the

Deep-sea Drilling Project. vol. 26. U.S. Government Printing Office, Washington, D.C., pp. 745–769.

Herman, A., Spicer, R.A., 1997. New quantitative palaeoclimate data for the Late Cretaceous Arctic: evidence for a warm polar ocean. Palaeogeogr. Palaeoclimatol. Palaeoecol. 128, 227–251.

Hong, S.K., Lee, Y.I., 2012. Evaluation of atmospheric carbon dioxide concentrations during the Cretaceous. Earth Planet. Sci. Lett. 327, 23–28.

Huber, B.T., 1988. Upper Campanian-Paleocene foraminifera from the James Ross Island region (Antarctic Peninsula). In: Feldmann, R.M., Woodburne, M.O. (Eds.), Geology and Paleontology of Seymour Island, Antarctica. vol. 169. Geological Society of America Memoir, pp. 163–251.

Huber, B.T., 1990. Maestrichtian planktonic foraminifer biostratigraphy of the Maud Rise (Weddell Sea, Antarctica): ODP Leg 113 Holes 689B and 690C. In: Barker, P.F., Kennett, J.P., Shipboard Scientific Party (Eds.), Proceedings of the Ocean Drilling Program, Scientific Results. vol. 113. Ocean Drilling Program, College Station, TX, pp. 489–513.

Huber, B.T., 1992. Upper Cretaceous planktic foraminiferal biozonation for the Austral Realm. Mar. Micropaleontol. 20, 107–128.

Huber, B.T., Leckie, R.M., 2011. Planktic foraminiferal species turnover across deep-sea Aptian/Albian boundary sections. J. Foraminifer. Res. 41, 53–95.

Huber, B.T., Hodell, D.A., Hamilton, C.P., 1995. Middle-late Cretaceous climate of the southern high latitudes: stable isotope evidence for minimal equator-to-pole thermal gradients. Geol. Soc. Am. Bull. 107 (10), 1164–1191.

Huber, B.T., Norris, R.D., MacLeod, K.G., 2002. Deep-sea paleotemperature record of extreme warmth during the Cretaceous. Geology 30, 123–126.

Huber, B.T., MacLeod, K.G., Gröcke, D., Kucera, M., 2011. Paleotemperature and paleosalinity inferences and chemostratigraphy across the Aptian/Albian boundary in the subtropical North Atlantic. Paleoceanography 26, PA4221. http://dx.doi.org/10.1029/2011PA002178.

Huber, B.T., Petrizzo, M.R., Young, J., Falzoni, F., Galiardoni, S., Bown, P.R., Wade, B.S., 2016. A new online taxonomic database for planktonic foraminifera. Micropaleontology 62, 429–438.

Jahren, A.H., Arens, N.C., Sarmiento, G., Guerrero, J., Amundson, R., 2001. Terrestrial record of methane hudrate dissociation in the Early Cretececous. Geology 29, 159–162.

Jarvis, I., Gale, A.S., Jenkyns, H.C., Pearsce, M.A., 2006. Secular variation in Late Cretaceous carbon isotopes: a new δ^{13}C carbonate reference curve for the Cenomanian–Campanian (99.6–70.6 Ma). Geol. Mag. 143, 561–608.

Jenkyns, H.C., 1980. Cretaceous anoxic events: from continents to oceans. J. Geol. Soc. Lond. 137, 171–188.

Jenkyns, H.C., 2010. Geochemistry of oceanic anoxic events. Geochem. Geophys. Geosyst. 11. http://dx.doi.org/10.01029/02009GC002788.

Jenkyns, H.C., Dickson, A.J., Ruhl, M., van den Boorn, S.H.J.M., 2017. Basalt–seawater interaction, the Plenus Cold Event, enhanced weathering and geochemical change: deconstructing Oceanic Anoxic Event 2 (Cenomanian–Turonian, Late Cretaceous). Sedimentology 64, 16–43.

Jiménez Berrocoso, A., MacLeod, K.G., Martin, E.E., Bourbon, E., Londoño, C.I., Basak, C., 2010. Nutrient trap for Late Cretaceous organic-rich black shales in the tropical North Atlantic. Geology 38, 1111–1114.

Johnston, F.K.B., Turchyn, A.V., Edmonds, M., 2011. Decarbonation efficiency in subduction zones: Implications for warm Cretaceous climates. Earth Planet. Sci. Lett. 303 (1–2), 143–152.

Jones, C.E., Jenkyns, H.C., Coe, A.L., Hesselbo, S.P., 1994. Strontium isotopic variations in Jurassic and Cretaceous seawater. Geochim. Cosmochim. Acta 58, 3061–3074.

Kemp, D.B., Robinson, S.A., Crame, J.A., Francis, J.E., Ineson, J., Whittle, R.J., Bowman, V.C., O'Brien, C., 2014. A cool temperate climate on the Antarctic Peninsula through the latest Cretaceous to early Paleogene. Geology 42, 583–586.

Kennedy, W.J., Gale, A.S., Huber, B.T., Petrizzo, M.R., Bown, P.R., Barchetta, A., Jenkyns, H.C., 2014. Integrated stratigraphy across the Aptian/Albian boundary at Col de Pré-Guittard (southeast France): A candidate Global Boundary Stratotype Section. Cretac. Res. 51, 248–259.

Kennedy, W.J., Gale, A.S., Huber, B.T., Petrizzo, M.R., Bown, P., Jenkyns, H.C., 2017. The Global Boundary Stratotype Section and Point (GSSP) for the base of the Albian Stage, of the Cretaceous, the Col de Palluel section. Arnayon, Drôme, France Episodes 40 (3), 177–188.

Kennett, J.P., Stott, L.D., Shipboard Scientific Party, 1990. Proteus and Proto-Oceanus: Ancestral Paleogene oceans as revealed from Antarctic stable isotopic results; ODP Leg 113. In: Barker, P. F, Kennett J P (Eds.), Proceedings of the Ocean Drilling Program, Scientific Results. 113. Ocean Drilling Program, College Station, Texas, pp. 865–880.

Kennett, J.P., Stott, L.D., 1991. Abrupt deep-sea warming, palaeoceanographic changes and benthic extinctions at the end of the Palaeocene. Nature 353, 225–229.

Kim, S.-T., O'Neil, J.R., 1997. Equilibriaum and nonequilibrium oxygen isotope effects in synthetic carbonates. Geochim. Cosmochim. Acta 61, 3461–3475.

Krasheninnikov, V.A., Basov, I.A., 1983. Stratigraphy of Cretaceous sediments of the Falkland Plateau based on planktonic foraminifers, Deep-sea Drilling Project, Leg 71. In: Ludwig, W.J., Krasheninnikov, V.A., Shipboard Scientific Party (Eds.), Initial Reports of the Deep-sea Drilling Project. vol. 71. U.S. Government Printing Office, Washington, D.C., pp. 789–820.

Ladant, J.-B., Donnadieu, Y., 2016. Palaeogeographic regulation of glacial events during the Cretaceous supergreenhouse. Nat. Commun. 7, 12771.

Larson, R.L., 1991a. Geological consequences of superplumes. Geology 19, 963–966.

Larson, R.L., 1991b. Latest pulse of Earth: evidence for a mid-Cretaceous superplume. Geology 19, 547–550.

Linnert, C., Robinson, S.A., Lees, J.A., Bown, P.R., Perez-Rodriguez, I., Petrizzo, M.R., Falzoni, F., Littler, K., Arz, J.A., Russell, E.E., 2014. Evidence for global cooling in the

Late Cretaceous. Nat. Commun. 5, 1–7.

Ludwig, W.J., Krasheninnikov, V.A., Shipboard Scientific Party, 1983. Initial Reports of the Deep-sea Drilling Project. vol. 71. U.S. Government Printing Office, Washington, D.C., pp. 1187.

Lunt, D.J., Farnsworth, A., Loptson, C., Foster, G.L., Markwick, P., O'Brien, C.L., Pancost, R.D., Robinson, S.A., Wrobel, N.E., 2016. Palaeogeographic controls on climate and proxy interpretation. Clim. Past 12, 1181–1198.

Macellari, C.E., 1988. Stratigraphy, sedimentology and paleoecology of Late Cretaceous/Paleocene shelf-deltaic sediments of Seymour Island (Antarctic Peninsula). In: Feldmann, R.M., Woodburne, M.O. (Eds.), Geology and Paleontology of Seymour Island, Antarctica. Geol. Soc. America, Memoir Series, vol. 169. pp. 25–53.

Mackensen, A., Ehrmann, W.U., 1992. Middle Eocene through early Oligocene climate history and paleoceanography in the Southern Ocean: stable oxygen and carbon isotopes from ODP sites on Maud Rise and Kerguelen Plateau. Mar. Geol. 108, 1–27.

MacLeod, K.G., Huber, B.T., 1996. Reorganization of deep ocean circulation accompanying a Late Cretaceous extinction event. Nature 380, 422–425.

MacLeod, K.G., Huber, B.T., 2001. The Maastrichtian record at Blake Nose (western North Atlantic) and implications for global palaeoceanographic and biotic changes. Lond. Geol. Soc. Lond. Western North Atlantic Palaeogene Cretaceous Palaeoceanogr. 183, 111–130 117 figures.

MacLeod, K.G., Huber, B.T., Isaza-Londoño, C., 2005. North Atlantic warming during global cooling at the end of the Cretaceous. Geology 33, 437–440.

MacLeod, K.G., Martin, E.E., Blair, S.W., 2008. Nd isotopic excrsion across Cretaceous ocean anoxic event 2 (Cenomanian-Turonian) in the tropical North Atlantic. Geology 36, 811–814.

MacLeod, K.G., Huber, B.T., Jiménez Berrocoso, A., Wendler, I., 2013. A stable and hot Turonian without glacial δ^{18}O excursions indicated by exquisitely preserved Tanzanian foraminifera. Geology 41, 1083–1086.

MacLeod, K.G., Quinton, P.C., Bassett, D.J., 2017. Warming and increased aridity during the earliest Triassic in the Karoo Basin, South Africa. Geology 45, 483–486.

Martin, E.E., MacLeod, K.G., Berrocoso, A.J., Bourbon, E., 2012. Water mass circulation on Demerara Rise during the Late Cretaceous based on Nd isotopes. Earth Planet. Sci. Lett. 327, 111–120.

Martin, J.E., Amiot, R., Lécuyer, C., Benton, M.J., 2014. Sea surface temperature contributes to marine crocodylomorph evolution. Nat. Commun. 5, 1–7.

Matthews, K.J., Seton, M., Muller, D.W., 2012. A global scale plate reorganization event at 105–100 Ma. Earth Planet. Sci. Lett. 355–356, 283–298.

McArthur, J.M., Howarth, R.J., Shields, G.A., 2012. Strontium isotope stratigraphy. In: Gradstein, F.M., Ogg, J.G., Schmitz, M.D., Ogg, G.M. (Eds.), The Geologic Time Scale. Elsevier B.V., Amsterdam, pp. 127–144.

Miller, K.G., Fairbanks, R.G., Mountain, G.S., 1987. Tertiary oxygen isotope synthesis, sea level history, and continental margin erosion. Paleoceanography 2, 1–19.

Miller, K.G., Barrera, E., Olsson, R.K., Sugarman, P.J., Savin, S.M., 1999. Does ice drive early Maastrichtian eustasy? Geology 27, 783–786.

Miller, K.G., Sugarman, P.J., Browning, J.V., Pekar, S.F., Katz, M.E., Cramer, B.S., Monteverde, D., Uptegrove, J., McLaughlin, J., Baxter, S.J., Aubry, M.-P., Olsson, R.K., Van Sickel, B., Metzger, K., Feigenson, M.D., Tiffin, S., McCarthy, F., 2003. Ocean view site. In: Miller, K.G., Sugarman, P.J., Browning, J.V., Shipboard Scientific Party (Eds.), Proceedings of the Ocean Drilling Program, Initial Reports. vol. 174AX (Suppl.). Ocean Drilling Program, College Station, Texas, pp. 1–72 (CD-ROM).

Miller, K.G., Sugarman, P.J., Browning, J.V., Kominz, M.A., Olsson, R.K., Feigenson, M.D., Hernández, J.C., 2004. Upper Cretaceous sequences and sea-level history. Geol. Soc. Am. Bull. 116, 368–393.

Miller, K.G., Wright, J.D., Browning, J.V., 2005. Visions of ice sheets in a greenhouse world. Mar. Geol. 217, 215–231.

Moiroud, M., Pucéat, E., Donnadieu, Y., Bayon, G., Guiraud, M., Voigt, S., Deconinck, J.-F., Monna, F., 2016. Evolution of neodymium isotopic signature of seawater during the Late Cretaceous: Implications for intermediate and deep circulation. Gondwana Res. 36, 503–522.

Moriya, K., Wilson, P.A., Friedrich, O., Erbacher, J., Kawahata, H., 2007. Testing for ice sheets during the mid-Cretaceous greenhouse using glassy foraminiferal calcite from the mid-Cenomanian tropics on Demerara Rise. Geology 35, 615–618.

Müller, R.D., Seton, M., Zahirovic, S., Williams, S.E., Matthews, K.J., Wright, N.M., Shephard, G.E., Maloney, K.T., Barnett-Moore, N., Hosseinpour, M., Bower, D.J., Cannon, J., 2016. Ocean basin evolution and global-scale plate reorganization events since Pangea breakup. Annu. Rev. Earth Planet. Sci. 44 (1), 107–138.

Murphy, D.P., Thomas, D.J., 2012. Cretaceous deep-water formation in the Indian sector of the Southern Ocean. Paleoceanography 27, PA1211. http://dx.doi.org/10.1029/2011PA002198.

O'Brien, C.L., Robinson, S.A., Pancost, R.D., Sinningeh Damsté, J.S., Schoulten, S., Lunt, D.J., Alsenz, H., Bornemann, A., Bottini, C., Brassell, S.C., Farnsworth, A., Forster, A., Huber, B.T., Inglis, G.N., Jenkyns, H.C., Linnert, C., Littler, K., Markwick, P., McAnena, A., Mutterlose, J., Naafs, B.D.A., Püttmann, W., Sluis, A., van Helmond, N.A.G.M., Vellekoop, J., Wagner, T., Wrobel, N.E., 2017. Cretaceous sea-surface temperature evolution: Constraints from TEX$_{86}$ and planktonic foraminiferal oxygen isotopes. Earth Sci. Rev. 172, 224–247.

Ogg, J.G., Ogg, G.M., Gradstein, F.M., 2016. A Concise Geologic Time Scale 2016. Elsevier, Amsterdam.

Olivero, E.B., Gasparini, Z., Rinaldi, C.A., Scasso, R., 1991. First record of dinosaurs in Antarctica (Upper Cretaceous, James Ross Island): palaeogeographic implications. In: Thomson, M.R.A., Crame, J.A., Thomson, J.W. (Eds.), Geological Evolution of Antarctica. Cambridge University Press, London, pp. 617–622.

Parrish, J.T., Spicer, R.A., 1988. Late Cretaceous terrestrial vegetation: A near-polar temperature curve. Geology 16, 22–25.

Parrish, J.T., Parrish, J.M., Hutchison, J.h., Spicer, R.A., 1989. Late Cretaceous vertebrate fossils from the North Slope of Alaska and implications for dinosaur ecology. Palaios

4, 299–300.

Pearson, P.N., 2012. Oxygen isotopes in foraminifera: overview and historical review. In: Ivany, L.C., Huber, B.T. (Eds.), Reconstructing Earth's Deep-Time Climate—The State of the Art in 2012, Paleontological Society Short Course, November 3, 2012. The Paleontological Society Papers. Vol. 18. Yale University, The Paleontological Society, pp. 1–38.

Perch-Nielsen, K., 1985. Mesozoic calcareous nannofossils. In: Bolli, H.M., Saunders, J.B., Perch-Nielsen, K. (Eds.), Plankton Stratigraphy. Cambridge University Press, Cambridge, pp. 329–426.

Petersen, S.V., Dutton, A., Lohmann, K.C., 2016. End-Cretaceous extinction in Antarctica linked to both Deccan volcanism and meteorite impact via climate change. Nat. Commun. 7. http://dx.doi.org/10.1038/ncomms12079.

Petrizzo, M.R., 2001. Late Cretaceous planktonic foraminifer from Kerguelen Plateau (ODP Leg 183): new data to improve the Southern Ocean biozonation. Cretac. Res. 22, 829–855.

Petrizzo, M.R., Falzoni, F., Premoli Silva, I., 2011. Identification of the base of the lower-to-middle Campanian Globotruncana ventricosa Zone: comments on reliability and global correlations. Cretac. Res. 32, 387–405.

Prentice, M.L., Matthews, R.K., 1991. Tertiary ice sheet dynamics: the snow gun hypothesis. J. Geophys. Res. 96, 6811–6827.

Pucéat, E., Lécuyer, C., Reisberg, L., 2005. Neodymium isotope evolution of NW Tethyan upper ocean waters throughout the Cretaceous. Earth Planet. Sci. Lett. 236, 705–720.

Pucéat, E., Donnadieu, Y., Naveau, P., Cappetta, H., Ramstein, G., Huber, B.T., Kriwet, J., 2007. Fish tooth δ^{18}O revising Late Cretaceous meridional upper ocean water temperature gradients. Geology 35, 107–110.

Railsback, L.B., Anderson, T.F., Ackerly, S.C., Cisne, J.L., 1989. Paleoceanographic modeling of temperature-salinity profiles from stable isotopic data. Paleoceanography 4, 585–591.

Ravizza, G., Norris, N.D., Blusztajn, J., Aubry, M.-P., 2001. An osmium isotope excursion associated with the late Paleocene thermal maximum: Evidence of intensified chemical weathering. Paleoceanography 16, 155–163.

Raymo, M.E., 1991. Geochemical evidence supporting T.C. Chamberlin's theory of glaciation. Geology 19, 344–347.

Raymo, M.E., Ruddiman, W.F., Froelich, P.N., 1988. Influence of late Cenozoic mountain building on ocean geochemical cycles. Geology 16, 649–653.

Renne, P.R., Sprain, C.J., Richards, M.A., Self, S., Vanderkluysen, L., Pande, K., 2015. State shift in Deccan volcanism at the Cretaceous-Paleogene boundary, possibly induced by impact. Science 350, 76–78.

Rich, T.H., Vickers-Rich, P., Gangloff, R.A., 2002. Polar Dinosaurs. Science 295, 979–980.

Robinson, S.A., Vance, D., 2012. Widespread and synchronous change in deep-ocean circulation in the North and South Atlantic during the Late Cretaceous. Paleoceanography 27. http://dx.doi.org/10.1029/2011PA002240.

Robinson, N., Ravizza, G., Coccioni, R., Peucker-Ehrenbrink, B., Norris, R., 2009. A high-resolution marine ^{187}Os/^{188}Os record for the late Maastrichtian: Distinguishing the chemical fingerprints of Deccan volcanism and the KP impact event. Earth Planet. Sci. Lett. 281, 159–168.

Robinson, S.A., Murphy, D.P., Vance, D., Thomas, D.J., 2010. Formation of "Southern Component Water" in the Late Cretaceous: Evidence from Nd-isotopes. Geology 38, 871–874.

Royer, D.L., Donnadieu, Y., Park, J., Kowalczyk, J., Goddéris, Y., 2014. Error analysis of CO$_2$ and O$_2$ estimates from the long-term geochemical model GEOCARBSULF. Am. J. Sci. 314, 1259–1283.

Savin, S.M., 1977. The history of the Earth's surface temperature during the past 100 million years. Ann. Rev. Earth Planet. Sci. 5, 319–355.

Savin, S.M., Douglas, R.G., Stehli, F.G., 1975. Tertiary marine paleotemperatures. Geol. Soc. Am. Bull. 86 (11), 1499–1510.

Shackleton, N.J., Kennett, J.P., 1975. Paleotemperature history of the Cenozoic and the initiation of Antarctic glaciation: Oxygen and carbon isotope analyses in DSDP Sites 277, 279, and 281. In: Kennett, J.P., Houtz, R.E. (Eds.), Initial Reports of the Deep-sea Drilling Project. 29. U.S. Government Printing Office, Washington, D.C., pp. 743–755.

Spiess, V., 1990. Late Cretaceous through Neogene deep-sea benthic foraminifers (Maud Rise, Weddell Sea, Antarctica). In: Barker, P.F., Kennett, J.P. (Eds.), Proceedings of the Ocean Drilling Program, Scientific Results. vol. 113. Ocean Drilling Program, College Station, TX, pp. 261–315.

Stoll, H.M., Schrag, D.P., 2000. High-resolution stable isotope records from the Upper Cretaceous rocks of Italy and Spain: Glacial episodes in a greenhouse planet? Geol. Soc. Am. Bull. 112, 308–319.

Stott, L.D., Kennett, J.P., 1990. The paleoceanographic and paleoclimatic signature of the Cretaceous/Paleogene boundary in the Antarctic: stable isotopic results from ODP Leg 113. In: Barker, P.F., Kennett, J.P. (Eds.), Proceedings of the Ocean Drilling Program, Scientific Results. 113. College Station, TX, Ocean Drilling Program, pp. 829–848.

Stott, L.D., Kennett, J.P., Shackleton, N.J., Corfield, R.M., 1990. The evolution of Antarctic surface waters during the Paleogene: Inferences from the stable isotopic composition of planktonic foraminifers, ODP Leg 113. In: Barker, P.F., Kennett, J.P. (Eds.), Shipboard Scientific Party, Proceedings of the Ocean Drilling Program, Scientific Results, Proceedings of the Ocean Drilling Program, Scientific Results. 113. pp. 849–863.

Takashima, R., Nishi, H., Huber, B.T., Leckie, R.M., 2006. Greenhouse world and the Mesozoic Ocean. Oceanography 19, 82–92.

Tarduno, J., Brinkman, D.B., Renne, P.R., Cottrell, R.D., Scher, H., Castillo, P., 1998. Evidence for extreme climatic warmth from Late Cretaceous Arctic vertebrates: Science. 282. pp. 2241–2244.

Thierstein, H.R., 1974. Calcareous nannoplankton-Leg 26, Deep-sea Drilling Project. In: Davies, T.A., Luyendyk, B.P. (Eds.), Initial Reports of the Deep Sea Drilling Project.

vol. 26. U. S. Govt. Printing Office, Washington, D. C., pp. 619–667.

Thomas, E., 1990. Late Cretaceous through Neogene deep-sea benthic foraminifers (Maud Rise, Weddell Sea, Antarctica). In: Barker, P.F., Kennett, J.P., Shipboard Scientific Party (Eds.), Proceedings of the Ocean Drilling Program, Scientific Results. vol. 113. Ocean Drilling Program, College Station, TX, pp. 571–594.

Thomas, E., Shackleton, N.J., 1996. The Paleocene-Eocene benthic foraminiferal extinction and stable isotope anomalies. In: Knox, R.W.O.B., Corfield, R., Dunay, R.E. (Eds.), Correlation of the early Paleogene in northwest Europe. 101. pp. 401–441.

Thomas, E., Barrera, E., Hamilton, N., Huber, B.T., Kennett, J.P., O'Connell, S.B., Pospichal, J.J., Spiess, V., Stott, L.D., Wei, W., Wise Jr., S.W., 1990. Upper Cretaceous-Paleogene stratigraphy of sites 689 and 690, Maud Rise (Antarctica). In: Barker, P.F., Kennett, J.P. (Eds.), Shipboard Scientific Party, Proceedings of the Ocean Drilling Project Scientific Results. 113. Ocean Drilling Program, College Station, TX, pp. 901–914.

Thomas, D.J., Korty, R.L., Huber, M., Schubert, J.A., Haines, B., 2014. Nd isotopic structure of the Pacific Ocean 70–30 Ma and numerical evidence for vigorous ocean circulation and ocean heat transport in a greenhouse world. Paleoceanography 29 (5), 454–469.

Tobin, T.S., Ward, P.D., Steig, E.J., Olivero, E.B., Hilburn, I.A., Mitchell, R.N., Diamond, M.R., Raub, T.D., Kirschvink, J.L., 2012. Extinction patterns, δ^{18}O trends, and magnetostratigraphy from a southern high-latitude Cretaceous–Paleogene section: Links with Deccan volcanism. Palaeogeogr. Palaeoclimatol. Palaeoecol. 350–352, 180–188.

Vail, P. R., Mitchum, R. M., Jr., and Thomson, S., III, 1977, Seismic stratigraphic and global changes of sea level, part 4: Global cycles of relative changes of sea level, *in* Payton, C. E., ed., Seismic Stratigraphy-Applications to Hydrocarbon Exploration, vol. 26: Tulsa, OK, American Association of Petroleum Geologists Memoir, p. 83–97.

Vandermark, D., Tarduno, J.A., Brinkman, D.B., 2007. A fossil champsosaur population from the high Arctic: Implications for Late Cretaceous paleotemperatures. Palaeogeogr. Palaeoclimatol. Palaeoecol. 248, 49–59.

Voigt, S., Jung, C., Friedrich, O., Frank, M., Teschner, C., Hoffmann, J., 2013. Tectonically restricted deep-ocean circulation at the end of the Cretaceous greenhouse. Earth Planet. Sci. Lett. 369–370, 169–177.

Watkins, D.K., Bergen, J.A., 2003. Late Albian adaptive radiation in the calcareous nannofossil genus *Eiffelithus*: Micropaleontology, v. 49. pp. 231–252.

Watkins, D.K., Wise, S.W.J., Pospichal, J.J., Crux, J.A., 1996. Upper Cretaceous calcareous nannofossil biostratigraphy and paleoceanography of the Southern Ocean, Microfossils and Oceanic Environments; British Micropalaeontological Society, University of Wales, p. pp. 355–381.

Westerhold, T., Röhl, U., Donner, B., McCarren, H.K., Zachos, J.C., 2011. A complete high-resolution Paleocene benthic stable isotope record for the central Pacific (ODP Site 1209. Paleoceanography 26 http://dx.doi.org/10.1029/2010PA002092. PA2216.

Wendler, I., Huber, B.T., MacLeod, K.G., Wendler, J.E., 2013. Stable oxygen and carbon isotope systematics of exquisitely preserved Turonian foraminifera from Tanzania - Understanding isotopic signatures in fossils. Mar. Micropaleontol. 102, 1–33.

Wilf, P., Johnson, K.R., Huber, B.T., 2003. Correlated terrestrial and marine evidence for global climate changes before mass extinction at the Cretaceous-Paleogene boundary. In: Proceedings of the National Academy of Sciences. 100. pp. 599–604.

Wise Jr., S.W., 1983. Mesozoic and Cenozoic nannofossils recovered by Deep-sea Drilling Project Leg 71 in the Falkland Plateau region, Southwest Atlantic Ocean. In: Ludwig, W.J., Krasheninnikov, V.A. (Eds.), Initial Reports of the Deep-sea Drilling Project. 71. U.S. Government Printing Office, Washington, D.C., pp. 481–550.

Wise Jr., S.W., Breza, J.R., Harwood, D.M., Wei, W., Zachos, J.C., 1992. Paleogene glacial history of Antarctica in light of ODP Leg 120 drilling results. In: Wise Jr.S.W., Schlich, R. (Eds.), Shipboard Scientific Party, Proceedings of the Ocean Drilling Project, Scientific Results, Volume 120: College Station, TX, Ocean Drilling Program, pp. 1001–1030.

Zachos, J.C., Breza, J., Wise, S.W.J., 1992. Earliest Oligocene icesheet expansion on East Antarctica: stable isotope and sedimentological data from Kerguelen Plateau: Geology, v. 20, p. pp. 569–573.

Zheng, X.-Y., Jenkyns, H.C., Gale, A.S., Ward, D.J., 2013. Changing ocean circulation and hydrothermal inputs during Ocean Anoxic Event 2 (Cenomanian–Turonian): Evidence from Nd-isotopes in the European shelf sea. Earth Planet. Sci. Lett. 375, 338–348.

Zhou, J., Poulsen, C.J., Pollard, D., White, T.S., 2008. Simulation of modern and middle Cretaceous marine d18O with an ocean-atmosphere general circulation model. Paleoceanography 23 (PA3223). http://dx.doi.org/10.1029/2, 1990" has not been found in the reference list. Please supply full details for this reference. Q15 Citation "Kennett and Stott, 1991" has not been found in the reference list. Please supply full details for this reference. Q16 The citation "Ladant et al., 2016" has been changed to "Ladant and Donnadieu, 2016" to match the author name/date in the reference list. Please check if the change is fine in this occurrence and modify the subsequent occurrences, if necessary. Q17 The citation "Larson and Erba, 1999" has been changed to "Larson, 1991a, b" to match the author name/date in the reference list. Please check if the change is fine in this occurrence and modify the subsequent occurrences, if necessary. 008PA001596.

Zhou, J., Poulsen, C.J., Rosenbloom, N.A., Shields, C., Briegleb, B., 2012. Vegetation-climate interactions in the warm mid-Cretaceous. Clim. Past 8, 565–576.